Rapid purification and metabolomic profiling of synaptic vesicles from mammalian brain

Lynne Chantranupong[1], Jessica L. Saulnier[1], Wengang Wang[1], Drew R. Jones[2]*, Michael E. Pacold[3]*, Bernardo L. Sabatini[1]

*these authors contributed equally

[1]Department of Neurobiology, Howard Hughes Medical Institute, Harvard Medical School, Boston, United States;
[2]New York University School of Medicine, Metabolomics Core Resource Laboratory at NYU Langone Health, New York, United States
[3]Department of Radiation Oncology, New York University Langone Medical Center, New York, United States

Abstract

Neurons communicate by the activity-dependent release of small-molecule neurotransmitters packaged into synaptic vesicles (SVs). Although many molecules have been identified as neurotransmitters, technical limitations have precluded a full metabolomic analysis of synaptic vesicle content. Here, we present a workflow to rapidly isolate SVs and to interrogate their metabolic contents at a high-resolution using mass spectrometry. We validated the enrichment of glutamate in SVs of primary cortical neurons using targeted polar metabolomics. Unbiased and extensive global profiling of SVs isolated from these neurons revealed that the only detectable polar metabolites they contain are the established neurotransmitters glutamate and GABA. Finally, we adapted the approach to enable quick capture of SVs directly from brain tissue and determined the neurotransmitter profiles of diverse brain regions in a cell-type specific manner. The speed, robustness, and precision of this method to interrogate SV contents will facilitate novel insights into the chemical basis of neurotransmission.

Introduction

Critical to the function of the brain are neurotransmitters, a diverse class of small molecules that act as chemical messengers between neurons. Neurotransmitters are stored in synaptic vesicles (SVs), membrane-bound organelles located within presynaptic axon terminals and whose activity-dependent release is essential for proper transmission of information within the brain (Jahn and Südhof, 1994). Upon electrical excitation of a neuron via action potentials, SVs rapidly fuse with the membrane to release their neurotransmitters, which are detected by transmembrane receptors on a postsynaptic neuron (Südhof, 2013; Traynelis et al., 2014) . This binding event can trigger diverse consequences to the postsynaptic neuron, depending on the identity of the neurotransmitter and the receptors to which it binds. Whereas some neurotransmitters cause acute electrical activation or inhibition of a neuron by opening ion channels, others result in longer-term modulation of its signaling network by activating G-protein coupled receptors (Nicoll et al., 1990). Thus, the functional contribution of a neuron to a circuit is defined by the neurotransmitters it releases and the postsynaptic cells that it contacts.

Although neurotransmitters were discovered more than a century ago, our understanding of what molecules are used as neurotransmitters and how they change during life is likely incomplete. Neurons were classically believed to release only one fast-acting neurotransmitter, whose identity was fixed throughout the lifetime of the neuron (Strata and Harvey, 1999). However, neurons in many brain regions have recently been discovered to release multiple neurotransmitters (Hnasko and Edwards, 2012; Jonas et al., 1998; Root et al., 2014; Shabel et al., 2014; Tritsch et al., 2012). Further increasing the complexity, these neurotransmitters may be packaged within the same or different SV pools or released from distinct axon terminals (Hnasko and Edwards, 2012; Saunders et al., 2015). Each possibility has unique effects on functionality and plasticity within circuits. In addition, neurons in the developing and mature brain have been found to lose, add, or switch the neurotransmitters they release in an activity-dependent manner (Dulcis et al., 2013; Spitzer, 2012). Finally, there exist synapses in which the neurotransmitters released remain unknown. Although many neurons have been found to contain the machinery to synthesize and potentially release neurotransmitters, it remains to be established if this release occurs and whether it has functional consequences (Mickelsen et al., 2017; Trapp and Cork, 2020). Altogether, these discoveries greatly expand how neurotransmitters control brain circuitry and reveal the complexities that remain to be deduced.

Current techniques to infer the neurotransmitter identity of neurons rely on detecting the molecular machinery involved in synthesizing, packaging, or binding to neurotransmitters; however, these methods have several caveats which limit their applicability. Low mRNA and protein expression levels coupled with poor reagents for detection lead to false negatives and inaccurate conclusions (Hnasko and Edwards, 2012). Moreover, these approaches do not account for neurons that use unknown

neurotransmitters or non-canonical pathways for neurotransmitter synthesis (Kim et al., 2015; Tritsch et al., 2012). In addition, the substrate specificities for many neurotransmitter receptors and vesicular transporters remain unclear (Yelin and Schuldiner, 1995). Alternatively, neurotransmitter identity is often inferred by pharmacological analysis of the receptors that mediate postsynaptic effects; for instance, a synaptic current is assumed to be induced by GABA release if it is blocked by an antagonist of ionotropic GABA receptors. However, many neurotransmitter receptors can be activated or allosterically modulated by diverse sets of small molecules that are found within cells, making this pharmacological approach difficult to interpret (Macdonald, 1994; Patneau and Mayer, 1990).

Many of these concerns can be addressed by direct profiling of SV contents using mass spectrometry (MS), a powerful tool that identifies diverse metabolites in a systematic, sensitive and robust manner (Patti et al., 2012). Indeed, MS has greatly expanded our understanding of organellar biology by providing insight into their rich and dynamic metabolomes (Abu-Remaileh et al., 2017; Chen et al., 2016). To accurately profile the metabolic contents of SVs, quick and specific purification methods for SVs are required. However, current protocols are optimized for proteomic characterizations of SVs and require several hours to days to complete, during which the activity of transporters and biosynthetic enzymes may alter the contents of purified SVs (Ahmed et al., 2013; Chen et al., 2016). More importantly, these protocols are difficult to apply to specific neuronal populations in complex tissue.

To overcome these caveats, we developed a method to rapidly immunopurify SVs from both cultured mouse neurons and intact mouse brains within half an hour. In combination, we employed MS to directly and comprehensively interrogate the metabolic contents of SVs. With this workflow, we characterized the neurotransmitter profiles for diverse brain regions in a cell-type specific manner. This method will serve as a foundation to discover and understand the diverse ways that neurons communicate with one another to control brain function.

Results

A method for rapid and specific capture of SVs from cultured neurons

In developing a method to dramatically reduce SV purification times while maintaining purity, we were inspired by immunoprecipitation (IP)-based workflows for organellar isolation which are highly specific and do not require time-consuming differential centrifugation techniques classically used to isolate organelles (Abu-Remaileh et al., 2017; Chen et al., 2016; Ray et al., 2020). We developed SV-Tag, a construct in which a hemagglutinin (HA) tag is fused to the C-terminus of synaptophysin, an SV-specific, integral membrane protein and an ideal candidate to tag due to its ubiquitous presence and high abundance on SVs (Figure 1A) (Takamori et al., 2006). In addition, we appended a tdTomato sequence

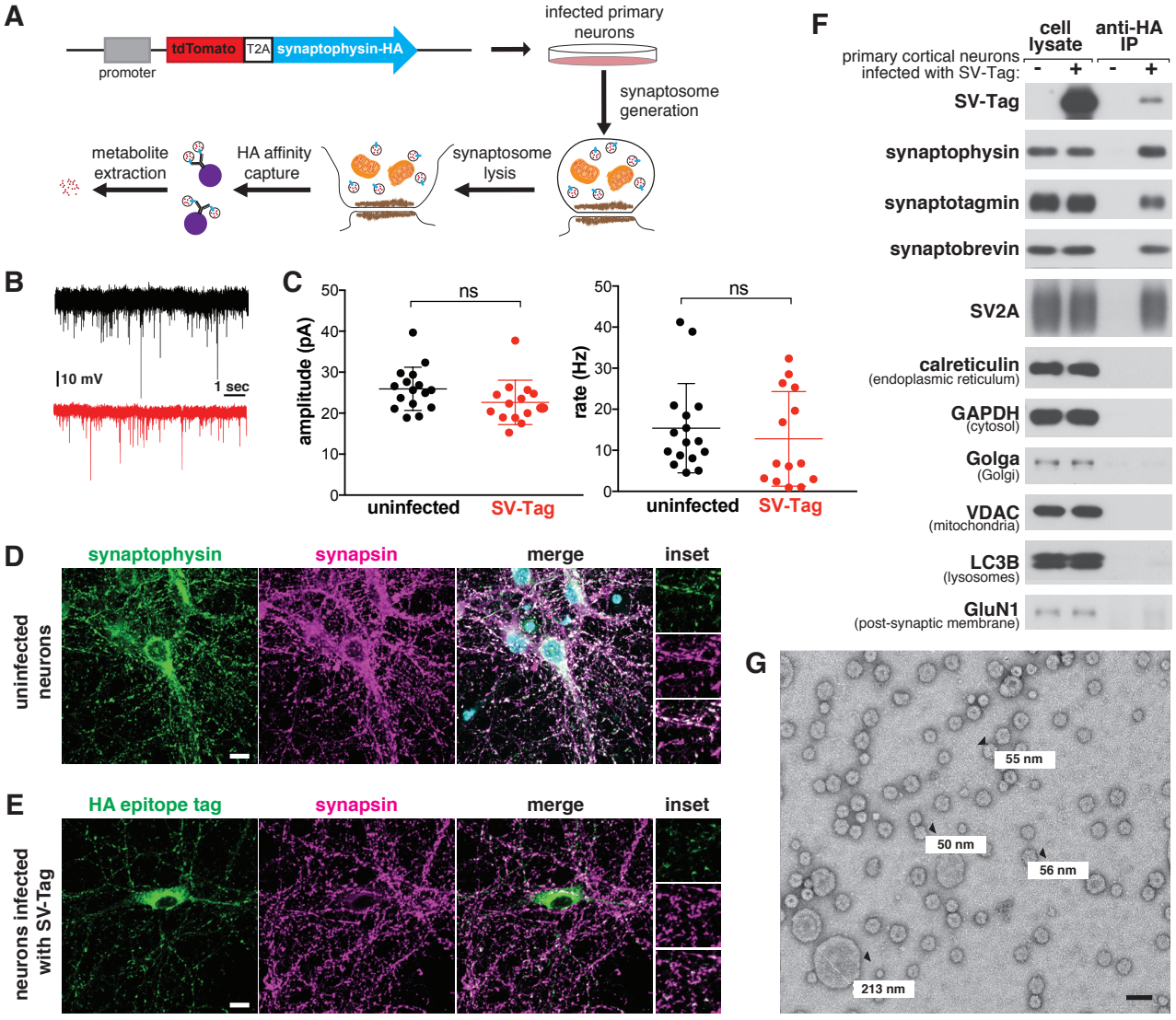

Figure 1: A method for rapid and specific isolation of synaptic vesicles from mouse primary cortical cultures (**A**) Construct design for tagging synaptic vesicles and schematic of the workflow used to isolate synaptic vesicles. (**B**) Representative trace of mEPSC responses from uninfected neurons (black) and neurons infected with SV-Tag (red). (**C**) Summary of the average amplitude (± standard deviation (std)) and rate of mEPSC responses from uninfected neurons and neurons infected with SV-Tag (V_{hold} = -70mV, 1μM TTX, 10 μM gabazine). Non-significant p value = n.s. (**D**) Immunostaining of uninfected primary neurons for endogenous synaptophysin (green) and synapsin (magenta). Insets represent selected fields that were magnified 1.6X. Scale bars: 10 μm. (**E**) Immunostaining of infected primary neurons expressing SV-Tag (green) and synapsin (magenta) in. Insets represent selected fields that were magnified 1.6X. Scale bars: 10 μm. (**F**) Immunoblot analysis of protein markers for synaptic vesicles and indicated subcellular compartments in whole cell lysates, purified synaptic vesicles, and control immunoprecipitates. Lysates were prepared from neurons infected with lentivirus encoding SV-Tag. (**G**) Electron microscope image of vesicles isolated with the workflow. Values denote diameter of indicated particles, specified by black arrows. Scale bar: 100 nm

followed by a self-cleaving T2A sequence to allow quick identification of infected cells via florescence. This strategy has several advantages compared to using an antibody against endogenous synaptophysin to isolate SVs. First, the SV-Tag construct can be easily modified to express in genetically defined subpopulations, which is crucial given the heterogeneity of neurons and brain tissue. Furthermore, the HA antibody is highly specific, sensitive, and well-characterized. Finally, the SV-Tag strategy enables this method to be generalizable as the HA tag is easily appended to other proteins and is compatible with many other applications, including metabolic and proteomic studies (Chen et al., 2017; Huttlin et al., 2015).

Because our workflow relies on immuno-affinity purification of subcellular compartments labeled with an ectopically expressed construct, it is necessary to ensure that this fusion protein does not perturb neurotransmitter release and is properly localized to SVs. In cultured mouse cortical neurons, the expression of SV-Tag did not alter the amplitude nor the rate of intrinsic glutamate release from these cells, as determined by recording spontaneous miniature excitatory post synaptic currents (mEPSCs) at a holding potential of -70 mV in the presence of TTX and gabazine (Figure 1B-C). To assess the localization of SV-Tag, we compared its distribution to that of synapsin-1, a synaptic vesicle protein that prominently marks presynaptic boutons (Camilli et al., 1983). Although SV-Tag colocalizes with synapsin, a fraction of it is also detected in the soma in apparently synapsin-free areas (Figure 1E). In contrast, endogenous synaptophysin completely colocalizes with synapsin, with a small fraction of the signal in the perinuclear area (Figure 1D). We therefore pursued multiple optimization routes to improve the targeting of SV-Tag. We moved the HA tag to the N-terminus, lowered expression levels, tagged endogenous synaptophysin using CRISPR, tested other epitope tags (FLAG, GFP), and tagged other SV resident proteins (SV2A, VAMP2, synaptotagmin) (Figure S1A). Surprisingly, for all of these approaches the epitope tagged protein exhibited somatic localization comparable to that of SV-Tag (Figure S1A). This suggests that for recombinant SV proteins, it is difficult to achieve the correct level of expression to ensure that they are trafficked from the soma to the boutons. Alternatively, it could indicate that a population of endogenous synaptophysin is somatically localized but not accessible by the synaptophysin antibody. This latter hypothesis is supported by the appearance of a somatic pool of synaptophysin when an HA tag was introduced into the endogenous gene (Figure S1A, top row). Therefore, we decided to use our original synaptophysin-based SV-Tag construct, due to the advantages of synaptophysin being a protein that is easy to express, abundant, and ubiquitously present on SVs (Takamori et al., 2006).

Based on a series of classical SV purification methods (Camilli et al., 1983; Craige et al., 2004; Huttner et al., 1983; Nagy et al., 1976), we developed a workflow to immunoisolate SVs from cultured cortical neurons within 30 minutes, a substantial reduction in time compared to the multiple hours to days needed for classical methods (Figure 1A). First, we formed synaptosomes, which are isolated synaptic terminals (Figure S1C). Unlike direct cell lysis to release SVs, this process affords us a key advantage of separating and discarding the soma, along with its mislocalized SV-Tag. We isolated synaptosomes

within just seven minutes by optimizing the homogenization steps needed to generate synaptosomes and the speed and duration of spins that are necessary to separate unlysed cells from synaptosomes. ATP was added throughout the purification to maintain vATPase function, which establishes the proton gradient across the SV membrane that is necessary for the import of neurotransmitters and the maintenance of their levels within SVs (Burger et al., 1989). Following hypotonic lysis of the synaptosomes to release SVs, we immunoprecipitated SVs using HA antibodies conjugated to solid magnetic beads. The reduced porosity and magnetic properties of these beads enable cleaner, quicker capture compared to standard agarose beads, which can trap metabolite contaminants within their porous bead matrix (Chen et al., 2016). A series of high salt washes post-immunoprecipitation disrupted non-specific protein and metabolite interactions and further reduced contaminants. During our initial attempts to IP SVs, we used a triple HA tag. Although this was sufficient to capture SVs as assessed by immunoblotting, the yield was low (Figure S1B). We reasoned that additional repeats of the HA epitope would increase capture efficiency by enhancing the probability that the tag will encounter an antibody during the IP period. Indeed, an extended tag of nine tandem HA sequences increased the yield of SVs despite expressing at a lower level than the triple HA tag (Figure S1B).

To assess the quality and integrity of SVs isolated by this rapid procedure, we characterized the isolate remaining at the end of the purification for multiple key features of SVs. Using immunoblotting, we confirmed the enrichment of SV protein markers such as synaptotagmin and SV2A and the concomitant depletion of markers for other subcellular organelles (Figure 1F). We then used mass spectrometry to profile the proteome of isolated SVs in depth and found that the most significantly enriched proteins were SV resident proteins, including glutamate transporters, synaptobrevin, and vATPase subunits (Supplementary Table 1) (Figure S1D) (Gronborg et al., 2010; Takamori et al., 2006). Furthermore, transmission electron microscopy revealed that the majority of particles isolated from our workflow are homogeneous spheres of ~30-50 nm in diameter (Eshkind and Leube, 1995), as expected for SVs (Figure 1G). A minority of larger particles (>100 nm) are also present, which may be large dense core vesicles (Gondré-lewis et al., 2012) or contaminating organelles and cellular debris. Finally, SVs isolated with SV-Tag are comparable to those purified via lengthier, traditional differential centrifugation protocols, as assessed by immunoblot (Figure S1E) and electron microscopy (Figure S1F), albeit with a reduction in yield that comes as a tradeoff for the speed of isolation.

Although these analyses indicate we were able to enrich for SVs, they do not provide evidence that the SVs are intact, which is crucial for subsequent metabolite analysis. If the integrity of isolated SVs is not compromised, they should contain glutamate, the principal neurotransmitter of cultured cortical neurons (Beaudoin III et al., 2012). Using a luminescence-based assay to detect glutamate, we observed an enrichment of glutamate in isolated SVs compared to the material obtained when the same protocol was applied to uninfected neurons (Figure S1G). Importantly, glutamate was depleted upon treatment of

neurons with BafilomycinA (BafA), a vATPase inhibitor that dissipates the proton gradient of SVs that is essential for the import of glutamate into SVs (Bowman et al., 1988). Taken together, multiple lines of evidence demonstrate that our SV-Tag workflow enables rapid and specific high-affinity capture of intact SVs.

Targeted and global metabolite profile of SVs from cultured neurons

To interrogate the metabolite contents of SVs in a precise and robust manner, we initially used targeted gas chromatography-mass spectrometry (GC/MS), a method with high sensitivity for many analytes, low cost and ease of operation, all of which are important considerations for optimization studies (Beale et al., 2018). We selected a panel of amino acids to profile, which included bona fide neurotransmitters (glutamate and glycine) (Gundersen et al., 2005), a putative neurotransmitter (aspartate) (Fleck and Palmerv, 1993), and non-neurotransmitter amino acids to assess the cleanliness of our preps. To identify metabolites that are enriched in SVs, we compared the signal of metabolites present in HA immunoprecipitates from SV-Tag infected neurons versus the signal from immunoprecipitates of uninfected neurons, which served as a control for metabolites that non-specifically adhere to HA beads (Chen et al., 2017) (Supplementary Table 3). In primary cortical cultures, glutamate was the sole metabolite that was significantly enriched in SVs when compared to control (Figure 2A) and it was the only metabolite depleted by BafA treatment (Figure 2B), consistent with the excitatory and glutamatergic identity of these neurons. Importantly, non-neurotransmitter amino acids were not enriched, demonstrating that our SV preparations are of high purity as they lack contaminating metabolites. Of note, aspartate was not detected in these vesicles, suggesting that it does not function as a neurotransmitter in these cells. The same conclusion was reached via electrophysiological studies for hippocampal excitatory synapses (Herring et al., 2015).

To demonstrate the applicability of this method to profile other neuron types, we isolated SVs from inhibitory neuron cultures (Figure S2A), prepared from the medial ganglionic eminence (MGE) (Franchi et al., 2018). Unlike cortical cultures, these neurons are GABAergic, as evidenced by their expression of VGAT, a GABA transporter (Wojcik et al., 2006), and their lack of VGLUT1 protein, a glutamate transporter (Pines et al., 1992) (Figure S2B). Reflecting the differences in the neurotransmitter identities of cortical and MGE-derived neurons, GC/MS analysis revealed that SVs isolated from MGE cells are enriched for GABA but not glutamate, whereas the converse is observed for cortical cultures (Figure S2C). Highlighting the specificity of our method, MGE SVs were not significantly enriched for any other amino acids profiled. Thus, by combining the SV-Tag isolation workflow with GC/MS, we can successfully obtain neurotransmitter profiles of diverse neuron subtypes.

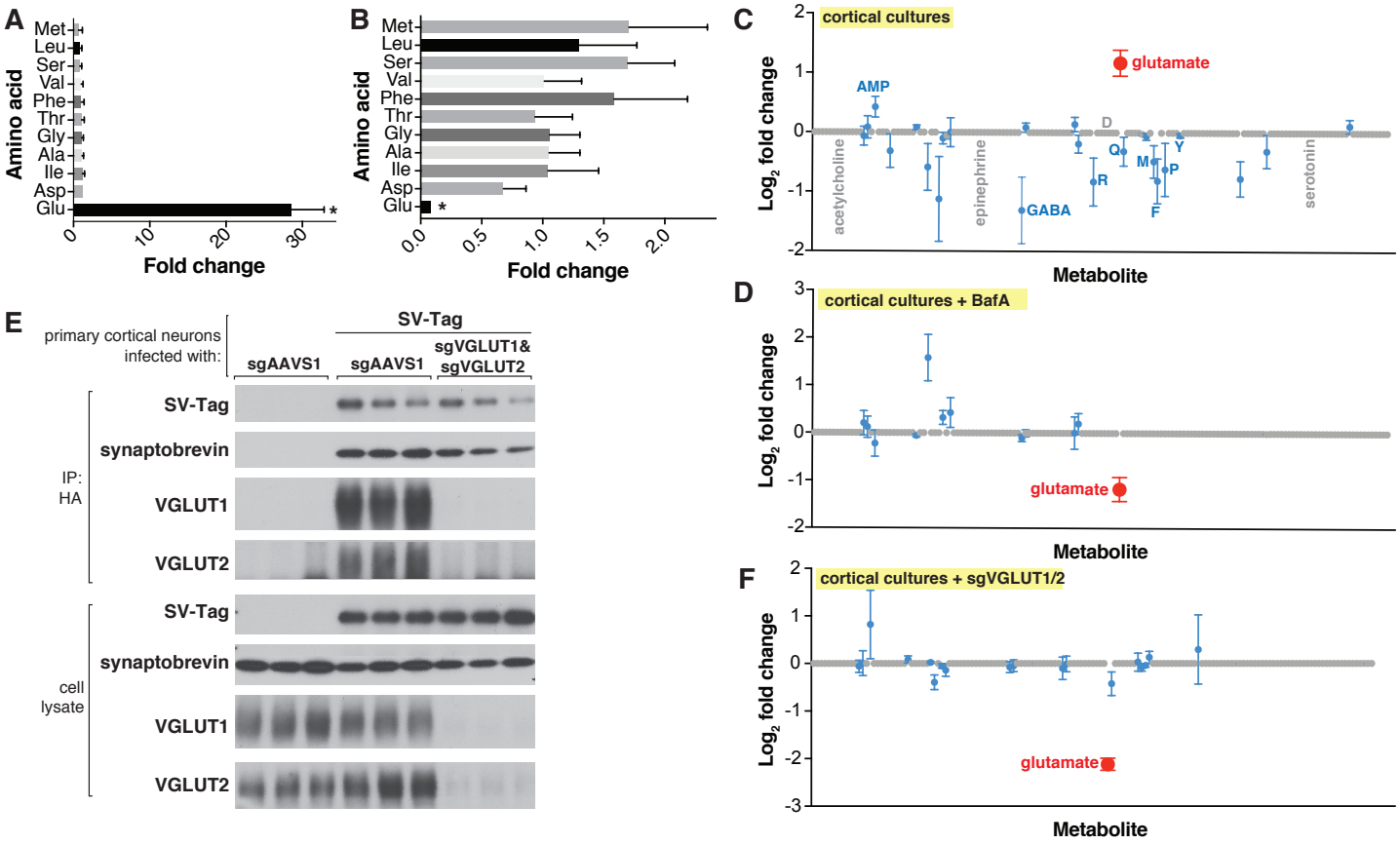

Figure 2: Targeted metabolite profile of purified synaptic vesicles from cultured neurons
(A) Fold change (mean ± standard error of the mean (SEM), n=3) of selected amino acids detected by GC/MS in purified SVs versus control IPs. Asterisk denotes a statistically significant difference (p value < 0.05) of the abundance of the indicated amino acid in SVs profiled from cells infected with SV-Tag compared to uninfected cells. (**B**) Effect of pretreatment of neurons with BafilomycinA on the abundance of selected amino acids in purified synaptic vesicles, as detected with GC/MS (mean ± SEM, n=3) (**C**) Relative abundance via LC/MS of 153 polar metabolites present in purified SVs derived from SV-Tag infected cells, compared to preps from uninfected cells (mean ± SEM, n = 3-4). Red indicates p value <0.05, blue indicates p value > 0.05, and gray indicates that the metabolite was undetected in all samples. Single letter codes annotate selected amino acids. Metabolites are listed in alphabetical order, and their corresponding identities can be found in Supplemental Table 2. (**D**) Effect of BafilomycinA on the presence of a panel of polar metabolites in purified synaptic vesicles profiled with LC/MS (mean ± SEM, n = 3-4). Fold changes are color coded using the same specifications as in (**C**). (**E**) Immunoblot analysis of neurons expressing control guides (sgAAVS1) or guides targeting glutamate transporters (sgVGLUT1 and sgVGLUT2). Lysates were prepared from neurons infected with lentivirus encoding the indicated constructs. Fold changes are color coded using the same specifications as in (C). (**F**) LC/MS metabolite profile of synaptic vesicles isolated from cells with glutamate transporter knockdown compared with control cells expressing the control guide.

Although GC/MS provides a strong starting point for analysis, it is limited in its capacity to detect a wide range of polar metabolites, due to the need for polar metabolite volatilization and separation on a GC column (Lei et al., 2011; Sobolevsky et al., 2003; Stenerson, 2011). Therefore, we transitioned to metabolomic analysis by liquid chromatography – high resolution mass spectrometry (LC/MS), which can detect a much broader range of metabolites with nanomolar sensitivity (Lei et al., 2011). We quantified the relative abundance of 153 polar compounds, which included neurotransmitters such as acetylcholine, serotonin, and epinephrine, as well as key molecules in metabolic pathways and subcellular compartments (Supplementary Table 2). Corroborating our earlier findings with GC/MS, glutamate was the sole detected metabolite that is significantly enriched within SV-Tag isolated SVs (Figure 2C) and depleted upon BafA treatment (Figure 2D) (Supplemental Table 5). All other metabolites were either undetected or detected at statistically insignificant levels. Reflecting the specificity of our workflow for isolating SVs, markers for other subcellular compartments were not enriched, including cystine, which is characteristic of lysosomes (Pisoni and Thoene, 1991), and aspartate and phosphocholine, which are the most enriched metabolites in mitochondria (Chen et al., 2016).

Because vATPase resides in other organelles (Kanazawa and Wada, 2000), the observation that its inhibition depletes glutamate is not sufficient to provide certainty that the glutamate detected is within SVs. To address this concern, we took advantage of the fact that glutamate is imported into SVs via glutamate transporters VGLUT1 and VGLUT2 (Takamori et al., 2001), which, unlike vATPase, are SV-specific proteins (Fremeau Jr et al., 2001). Reassuringly, CRISPR-mediated depletion of these transporters from cortical neurons by targeting the genes *Slc17a6* (VGLUT1) and *Slc17a7* (VGLUT2) significantly reduced glutamate levels from isolated SVs (Figure 2E, 2F). Taken together, these results demonstrate that our purification workflow isolates SVs of high purity and integrity which are compatible for robust and sensitive profiling with multiple MS methods.

Previous work has proposed that other polar molecules may function as neurotransmitters, including taurine, gamma-hydroxybutyrate, ß-alanine, and agmatine (Cash, 1994; Clarke and Haig, 1971; Kilb and Fukuda, 2017; Reis and Regunathan, 2000; Tiedje et al., 2010). To gain a more comprehensive and unbiased view of the SV metabolome, we performed a global metabolomics screen for polar metabolites (Figure 3A, 3B). The LC/MS runs were optimized for detection of a broad range of polar retentivities using a HILIC stationary phase and fast polarity switching MS method to capture analytes which ionize exclusively in positive or negative mode. Overall, we detected 2,724 representative features which were defined by an observed m/z (25 ppm) at a specific retention time (± 0.25 min) with a minimum intensity and signal to noise threshold (Supplemental Table 4).

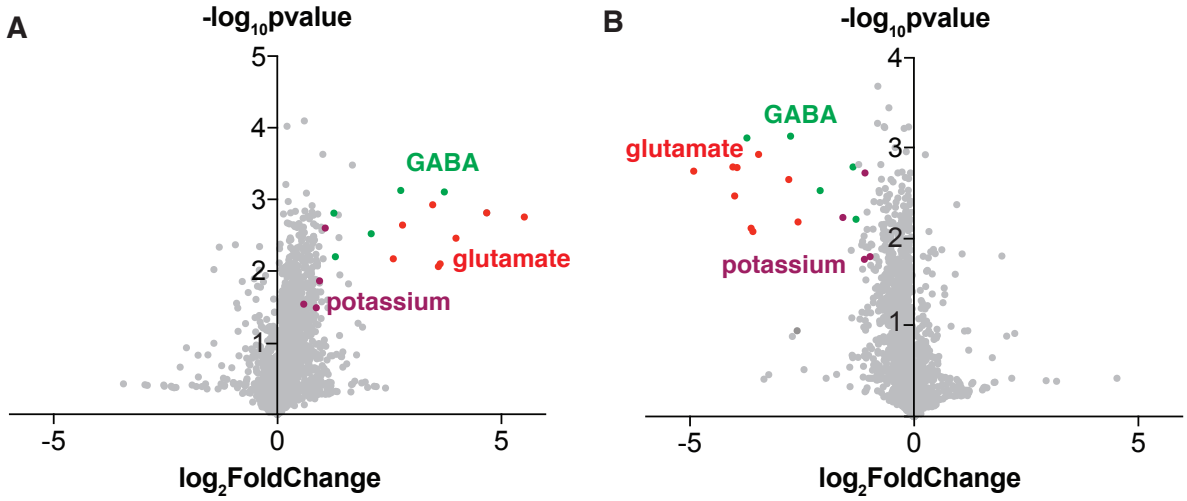

C

				SV-Tag IP/control IP		SV-Tag IP BafA/DMSO	
metabolite	polarity	m/z	retention time	log_2 fold change	pvalue	log_2 fold change	pvalue
glutamate	-	146.0447	11.53	5.52	0.0018	-4.92	0.0018
glutamate	+	148.0602	11.54	4.69	0.0015	-4.04	0.0016
glutamate (isotope)	+	149.0635	11.52	3.99	0.0035	-4.00	0.0035
glutamate	+	149.0601	11.52	4.68	0.0015	-3.95	0.0017
glutamate (sodium adduct)	+	170.0421	11.54	3.63	0.0079	-3.63	0.0079
glutamate (in-source fragment)	+	130.0497	11.54	3.60	0.0086	-3.60	0.0086
glutamate (CO_2 adduct)	+	190.0240	11.58	3.47	0.0012	-3.47	0.0012
glutamate (sodium adduct)	-	168.0269	11.53	2.79	0.0023	-2.79	0.0023
glutamate (in-source fragment)	+	84.0448	11.57	2.59	0.0067	-2.59	0.0067
GABA (in-source fragment)	+	87.0445	11.36	3.73	0.0008	-3.73	0.0008
GABA (in-source fragment)	+	86.0604	11.32	2.76	0.0007	-2.76	0.0007
GABA (M+1 isotope)	+	105.0741	11.34	2.09	0.0030	-2.09	0.0030
GABA	+	104.0708	11.35	1.37	0.0016	-1.37	0.0016
GABA (peak tail)	+	104.0708	11.37	1.30	0.0063	-1.30	0.0063
potassium	+	751.7706	22.88	0.87	0.0326	-1.59	0.0060
potassium	-	705.7961	22.86	0.59	0.0288	-1.11	0.0176
potassium	-	461.8357	23.21	0.94	0.0136	-1.10	0.0019
potassium	-	724.7686	22.86	0.45	0.0025	-0.98	0.0164

Figure 3: Unbiased polar metabolomics profile of purified synaptic vesicles from cultured cortical neurons

(**A**) Global polar metabolomics analysis via LC/MS of purified synaptic vesicles, compared to an IP from uninfected cells. Green indicates glutamate and its associated derivatives generated during the LC/MS run. Red indicates GABA and its derivatives. Purple indicates potassium. Each dot represents the average of three replicate samples. (**B**) Global polar metabolomics analysis on purified synaptic vesicles from Bafilomycin-treated versus DMSO treated neurons. Legend is same as in Figure 3A. (**C**) Summary of metabolites from global analysis which are significantly enriched in SV-Tagged SVs and significantly depleted by BafilomycinA treatment.

To identify SV-specific metabolites, we filtered for peaks that were significantly enriched by at least two-fold in SVs and concomitantly depleted by BafA by at least two-fold. To assign the peak identity of this small subset of features, we used a variety of manual approaches including spectral library search, accurate mass formula search and isotope fine structure. To our surprise, only three metabolites satisfied these criteria – glutamate, GABA, and potassium (Figure 3C, Supplemental Table 4). In these samples,

GABA likely originates from a minority population of interneurons in cultured cortical neurons, consistent with the low expression level of VGAT, the GABA transporter, observed in these cultures (Figure S2B). The variability of the number of GABAergic interneurons across different cortical culture preps likely contributes to the variation in the GABA levels detected across MS runs. In addition to GABA, we identified a peak that is associated with potassium, which arises from the putative pairing of this ion with carbonate ions in the LC buffers used in the IP/MS workflow. However, potassium is a ubiquitous component of multiple reagents and sample-to-sample fluctuations in their levels can contribute to altered potassium content. Follow-up studies using atomic absorption spectroscopy or inductively coupled plasma mass spectrometry (ICP-MS) will be necessary to establish how much potassium these SVs quantitatively contain, whether these weakly enriched potassium peaks are indeed internalized within SVs, and if they contribute to SV function.

Adaptation of the method for SV isolation and profiling from brain tissue

Given their relative homogeneity of neuron types and ease of preparation, cultured cortical neurons provide an ideal setting to optimize and test purification protocols. However, in the brain, molecularly and functionally distinct neurons are intermingled in an intricate and heterogeneous environment, and they rely on the uptake of extracellular metabolites found in this environment for neurotransmitter synthesis (Elsworth and Roth, 1997; Mathews and Diamond, 2003; Schousboe et al., 2013). To gain a more complete understanding of neurotransmission and potentially identify unknown endogenous neurotransmitters, it is necessary to profile SVs isolated from their native environment. We therefore adapted the method for use in brain tissue (Figure 4A). First, we expressed SV-Tag in the brain by transducing desired brain regions of mice via stereotaxic injections of adeno-associated viruses (AAV) encoding Cre-independent SV-Tag. To ensure neuron specific expression, the expression of SV-Tag was driven by the synapsin promoter (Kugler et al., 2003). SV-Tag readily expresses in diverse areas, as evidenced by the abundance of tdTomato positive neurons in targeted regions (Figure 4B). To ensure that SV-Tag does not impair neurotransmission *in vivo*, we examined synaptic transmission at well-characterized Schaffer collateral synapses between hippocampal CA3 and CA1 pyramidal cells (Figure S4A) (Jackman et al., 2014). Paired-pulse facilitation, which indicates changes in probability of release from presynaptic terminals, was assessed using pairs of closely spaced electrical stimuli (Figure S4B). Paired pulse ratios, measured at an inter-stimulus interval of 50 ms, were unaffected by SV-Tag expression in presynaptic neurons, which indicated that SV-Tag did not significantly alter neurotransmitter release probability at this synapse (Figure S4C).

Our initial attempts to isolate SVs from brain tissue using the same strategy developed for cultured neurons resulted in preps with poor yield and high background. This is not surprising given the complex structure and composition of brain tissue compared to cultured neurons, which grow as a

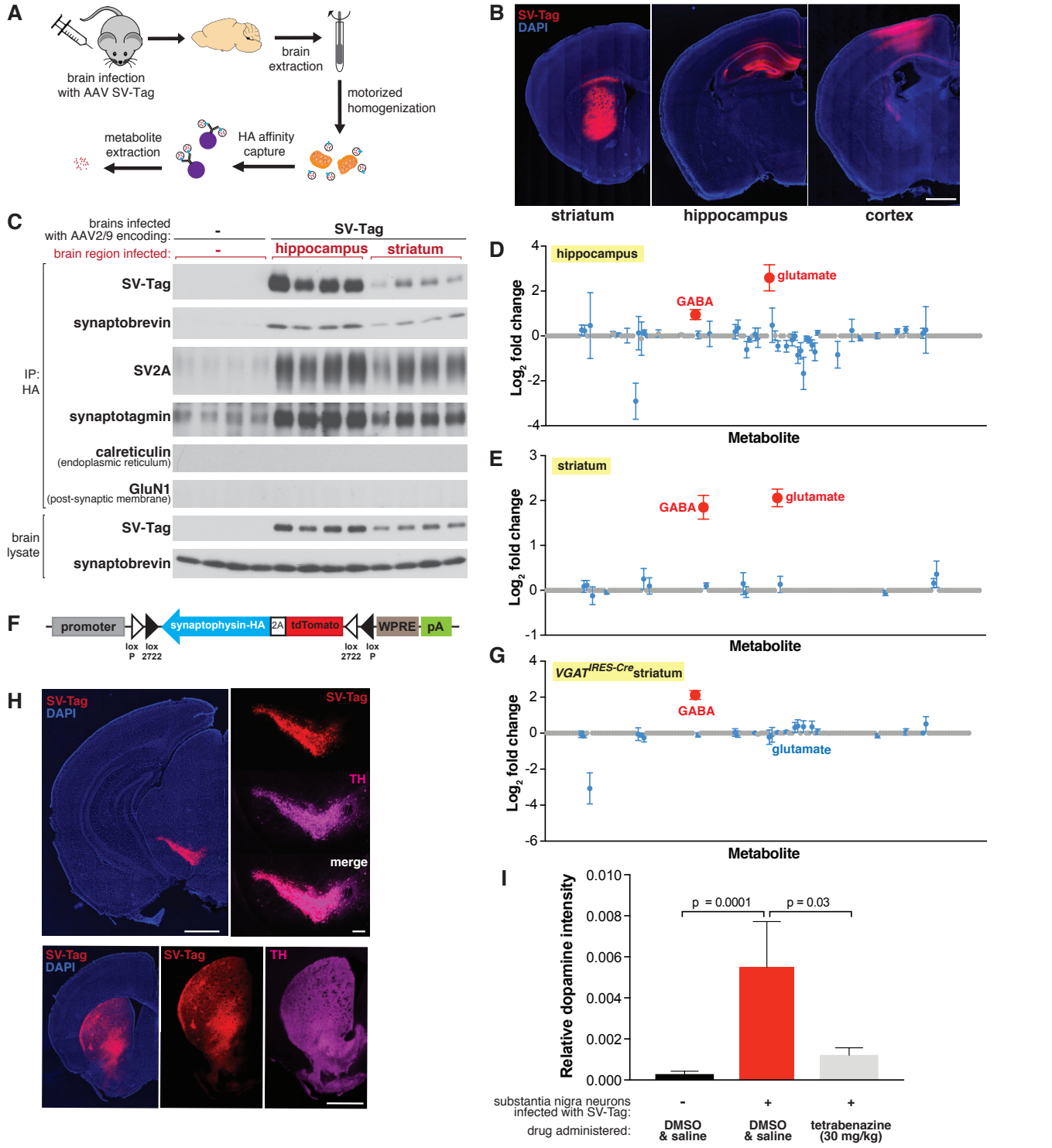

Figure 4: Adaptation of the workflow for rapid and specific isolation and metabolite profiling of synaptic vesicles directly from mouse brain tissue

(**A**) Schematic of the workflow used to isolate synaptic vesicles from mouse brain tissue. (**B**) Immunofluorescence images of coronal sections from wild type mouse brains transduced with SV-Tag in the indicated brain regions. Neurons are labeled with DAPI nuclear stain (blue) and SV-Tag (red). Scale bar = 1 mm. (**C**) Immunoblot analysis of indicated protein markers present in brain lysates, control

immunoprecipitates from uninfected brains, and HA immunoprecipitates from hippocampi and striatum that were infected with SV-Tag. (**D**) LC/MS profile of synaptic vesicles isolated from wild type mice brains infected with SV-Tag in hippocampus compared to a control IP from uninfected brains. (mean ± SEM, n=4). Color code and legend is the same as in Figure 2C. (**E**) LC/MS profile of synaptic vesicles isolated wild type mice brains infected with SV-Tag in striatum compared to uninfected brains. (mean ± SEM, n=4) (**F**) Construct design for expression of SV-Tag in neurons in a Cre-dependent manner. (**G**) LC/MS profile of synaptic vesicles isolated from *Slc32a1*$^{IRES\text{-}Cre/wt}$ (*VGAT*$^{IRES\text{-}Cre}$) mice brains infected with SV-Tag in striatum compared to uninfected brains. (mean ± SEM, n=4) (**H**) Coronal sections from a *Slc6a3*$^{IRES\text{-}Cre/wt}$ mouse transduced with Cre-dependent SV-Tag in dopaminergic neurons of the midbrain. Dopamine neurons are immunolabelled for tyrosine hydroxylase (TH, magenta), DAPI nuclear stain (blue) and SV-Tag (red). (**I**) Targeted LC/MS profiling of dopamine in synaptic vesicles isolated from *Slc6a3*$^{IRES\text{-}Cre/wt}$ mice transduced with Cre-dependent SV-Tag in dopaminergic neurons of the midbrain. Indicated mice were subjected to with saline injection or tetrabenazine injection intraperitoneally 2 hours prior to harvesting of synaptic vesicles.

homogeneous monolayer. To resolve these issues, we compared several lysis protocols for their efficiency in releasing SVs from neurons. Compared to forming and lysing synaptosomes, homogenizing the whole brain to immediately free SVs greatly improved yields (Figure S4D). Importantly, a rotarized homogenizer was necessary for effective and rapid lysis. The addition of a final five-minute high-salt incubation after the IP further reduced background contamination. In combination, these changes enabled SV isolation in under 30 minutes from diverse brain regions, including hippocampus, cortex, and striatum (Figure 4C, S4E). Moreover, SVs had minimal contamination of other subcellular organelles as demonstrated by immunoblot and electron microscope analyses (Figure 4C, S4E, S4F).

Utilizing the LC/MS workflow, we determined if our method is capable of distinguishing the content of SVs isolated from brain regions with different neurotransmitter profiles. We profiled SVs from the hippocampus, which is composed of roughly 90% glutamatergic pyramidal neurons and 10% GABAergic interneurons (Olbrich and Braak, 1985), and the striatum, which is comprised primarily of GABAergic cells (Yoshida and Precht, 1971). The metabolite profiles of hippocampal SVs are expected, with glutamate and GABA detected and $_{glutamate}$ being the more abundant neurotransmitter (Figure 4D). Similar to cortical culture SVs, no other metabolites other than these two known neurotransmitters were significantly present.

In contrast, striatal SVs were contaminated by a significant amount of glutamate. Because SV-Tag was expressed in a Cre independent manner in wild type mice, this could result from isolation of SVs from glutamatergic cortical neurons that lie above striatum and became infected with SV-Tag due to pipette withdrawal and viral leak or via retrograde transduction due to axonal-uptake of AAV. Alternatively, it could be due to contamination by cortical and thalamic glutamatergic terminals that heavily innervate the striatum. To distinguish between these possibilities, we generated a Cre-dependent construct of SV-Tag to enable cell type specific expression of this IP handle (Figure 4F) (Atasoy et al.,

2008). Striatal SVs from *Slc32a1*$^{IRES\text{-}Cre}$ mice, where SV-Tag expression is restricted to GABAergic neurons (Vong et al., 2011) and SVs from *Adora2a*^{Cre} mice, which restrict expression further to a subpopulation of GABAergic striatal neurons (Durieux et al., 2009)(Figure S4G), reveal the enrichment of GABA and the concomitant depletion of glutamate (Figure 4G and S4H). Altogether, these results indicate that cell-type specific expression of SV-Tag permits analysis of SV content on material isolated directly from complex brain tissue.

Thus far, we focused on the detection of neurotransmitters whose polar and stable nature is compatible for sensitive detection by LC/MS. However, some neurotransmitters are less stable, such as the rapidly oxidizable dopamine, a crucial neurotransmitter whose loss underlies debilitating motor ailments such as Parkinson's disease (Damier et al., 1999). To test if, despite its labile nature, our rapid SV isolation workflow enables detection of dopamine, we expressed SV-Tag in midbrain substantia nigra neurons of *Slc6a3*$^{IRES\text{-}Cre}$ mice where Cre recombinase is restricted to cells expressing DAT, the plasma membrane dopamine transporter. As has been previously demonstrated in the injection target, Cre-expressing cells in this mouse line match well with the population of neurons that express VMAT2, the vesicular dopamine transporter (Edwards, 1992; Lammel et al., 2015). We validated specificity of expression by immunohistochemical analysis, which indicated selective expression of SV-Tag in dopaminergic cells as seen by colocalization with tyrosine hydroxylase, a dopamine synthetic enzyme (Daubner et al., 2011) both in the soma and in axonal projections to striatum (Figure 4H). In a cohort of mice expressing SV-Tag, we administered tetrabenazine, a reversible inhibitor of VMAT2 (Erickson et al., 1996; Scherman et al., 1983), at a concentration validated to deplete dopamine from SVs in acute striatal slices (Figure S4I, S4J). Using a modified LC/MS method for the detection of dopamine, we find that substantia nigra SVs are enriched for dopamine and these stores are depleted by VMAT2 inhibition (Figure 4I). Taken together, we developed a workflow to enable rapid and specific purification of SVs directly from the brain, and to obtain the neurotransmitter profiles of a wide range of neurons in a cell-type specific manner.

Discussion

Neurons use a broad array of small molecules for fast chemical neurotransmission. The ability for different neuron classes to release different transmitters, along with the diversity of neurotransmitter specific postsynaptic receptors, enables complex and intermingled excitatory, inhibitory, and neuromodulatory trans-synaptic signaling in dense brain tissue. Furthermore, individual neurons are able to release multiple transmitters, sometimes releasing different neurotransmitters to different postsynaptic targets, as well as switch neurotransmitter identity in a developmental and activity dependent manner. This richness of neurotransmitter usage in the brain highlights the need for new methods to deduce neurotransmitter identity in an accurate and cell type specific manner. To address these needs, we

developed a workflow that combines high-affinity capture of epitope tagged SVs with MS-based metabolomics to comprehensively profile SV contents. We adapted our method to isolate SVs with speed and ease from both primary cultured neurons and genetically-defined neurons in brain tissue, which will allow complementary *in vitro* and *in vivo* studies in the future. Our study confirms the utility of combining IP and MS based methods to characterize organelles such as SVs, and underscores the importance of performing global analyses to draw unbiased conclusions of the metabolic contents of organelles.

Our analyses of polar metabolites in SVs profiled in this study reveal that these organelles have a minimal metabolic content and contain only previously recognized *bona fide* neurotransmitters, which is consistent with their primary role in neurotransmitter storage and release. We find that glutamatergic vesicles, isolated from either cultured neurons or directly from the brain, contain only glutamate and lack detectable amounts of other proposed neurotransmitters (such as aspartate). Indeed, untargeted analysis of polar metabolites failed to detect any additional molecule that was enriched within these vesicles. It is possible that non-polar molecules and ions could also be imported into SVs. Indeed, zinc has been proposed to function as a neurotransmitter at excitatory synapses (Vergnano et al., 2014). In future studies, it will be beneficial to modify our workflow to be compatible with MS methods for atomic ion and non-polar metabolite detection. In addition, further optimization of the immunocapture procedure to increase SV yields is necessary to utilize MS methods for atomic ion detection, which require high amounts of starting material.

Although our method is rapid and specific, improvements to increase its sensitivity for neurotransmitter detection, particularly from SVs isolated from the brain, would be beneficial, even for the detection of polar metabolites. We were able to identify dopamine in SVs from substantia nigra neurons, but not GABA and glutamate (Tritsch et al., 2016; Zhang et al., 2015), which are known to be released by these cells. In addition, we observed a robust GABA signal in SVs from striatal cells but did not detect acetylcholine, which is released by a small population of interneurons that reside in this region (Cox and Witten, 2019). As cholinergic neurons represent about 2% of striatal neurons (Zhou et al., 2002), this suggests a lower limit for the ability of our current protocol to detect minor neurotransmitters. The yield of SVs captured by our method and thus the detection limit would likely be increased by the use of a mouse line in which synaptophysin is endogenously tagged with HA in a conditional manner. This would permit more uniform and complete expression of SV-Tag in desired cells without ectopic overexpression, and thus increase SV yields and the consistency between preps. Furthermore, it would eliminate the need for tedious injections and facilitate greater turnaround time of experiments.

With a method to identify molecules that are enriched in SVs, we can pursue many intriguing questions and avenues. To determine whether specific molecules function as neurotransmitters, candidates can be easily profiled for their presence inside SVs using our workflow. For instance, in the

371 context of cultured neurons and the brain regions profiled in this study, neither aspartate nor taurine -
372 molecules long debated to be neurotransmitters - were enriched within SVs, thus bringing into question
373 their potential synaptic functions. Analysis in the hippocampus also failed to find evidence in support of
374 aspartate being a neurotransmitter (Herring et al., 2015). Another important avenue of research is
375 elucidating the function of transporter-like SV proteins such as SV2A and defining the substrate
376 specificities of promiscuous vesicular transporters, including VMAT2 (Lynch et al., 2004; Yelin and
377 Schuldiner, 1995). Loss of function experiments combined with global MS profiling will provide a powerful
378 strategy to interrogate how these proteins affect SV function. Finally, this method can be easily adapted
379 to other applications to resolve long-standing questions about SVs. For instance, the release properties of
380 SVs have long been known to be heterogeneous, and only a fraction of SVs known as the rapidly
381 releasable pool fuse upon electrical excitation of a neuron (Rizzoli and Betz, 2005). Proteomic profiling of
382 these different SV populations following immunoisolation could reveal the molecular basis for these
383 differences, which has long eluded researchers. In combination, these possibilities highlight the potential
384 of SV immunoisolation and metabolomics to address a wide range of biological questions.
385
386 In conclusion, the robustness and ease of our SV isolation and profiling methodology will serve as
387 a platform upon which we can gain a deeper understanding of the diverse ways that these organelles
388 control neurotransmission.

Materials and Methods

Preparation of neuronal cultures and drug treatments – Primary dissociated cortical cultures were prepared from cortices of E16-E18 embryos of CD-1 mice (Charles River stock # 022) as described (Sciarretta and Minichiello, 2010). Cultured inhibitory neurons were prepared from the MGE of E13-E14 mice. The following modifications were made to enhance culture health: tissue pieces were digested with papain (Worthington) instead of trypsin-EDTA, DNAse (Sigma) was added to break down released genomic DNA and aid in more efficient trituration, and 1 ml pipette tips (PipetOne) were used to titurate the tissue instead of fire polished pipettes for more consistency.

For immunohistochemistry experiments, ~1 million cells were plated onto 24-well plates pre-coated with Poly-D-Lysine (PDL) (Sigma) and laminin (Invitrogen). For biochemical isolations, 4-5 million cells were plated onto 10 cm plates pre-coated with Poly-D-Lysine (PDL) and laminin. Cells were maintained at 37°C and 5% CO_2. A third of the media was replaced every 3 days with fresh Neurobasal media, and 1 µM Arabinoside C (Sigma) was added on days in vitro (DIV) 5 to prevent overgrowth of astrocytes and microglia.

In experiments where SVs were isolated from BafilomycinA (BafA) treated neurons, prior to the isolation cells were treated for 2 hrs with 500 nM BafA (EMD Millipore) or the corresponding DMSO volume.

Lentiviral constructs and production – The following sense (S) and antisense (AS) oligonucleotides encoding the guide RNAs were cloned into a pLentiCRISPR vector (Addgene 52961):

sgAAVS1 (S): caccgTCCCCTCCACCCCACAGTG
sgAAVS1 (AS): aaacCACTGTGGGGTGGAGGGGAc

sgVGLUT1 (S): caccgGGAGGAGTTTCGGAAGCTGG
sgVGLUT1 (AS): aaacCCAGCTTCCGAAACTCCTCCc

sgVGLUT2 (S): caccgAGAGGACGGTAAGCCCCTGG
sgVGLUT2 (AS): aaacCCAGGGGCTTACCGTCCTCTc

Lentiviruses were produced by transfection of viral HEK-293T cells with SV-Tag in combination with the VSV-G envelope and CMV ΔVPR packaging plasmids. Twenty-four hours after transfection, the media was changed to fresh DMEM (Invitrogen) with 20% heat inactivated fetal bovine serum (Gemini BioProducts). Forty-eight hours after transfection, the virus containing supernatant was collected from the cells and centrifuged at 1000g for 5 minutes to remove cells and debris. Supernatants were stored for up to 1 week at 4°C and added to plated cortical neurons at DIV 3.

SV isolation from cortical cultures – Five million neurons plated on a 10 cm tissue culture dish at DIV12-14 were used for each immunoisolation. No more than two plates were processed at a time to increase the speed of isolation. All buffers and tubes used were prechilled on ice, with the exception of the metabolite extraction mix, which was kept on dry ice, and all steps were performed swiftly. Neurons were placed on ice to chill, rapidly rinsed with ice-cold phosphate buffered saline (PBS) to remove residual media, and gently scraped into 1 ml PBS. Cells were pelleted by a brief centrifugation step at 2400g for 40 seconds. The PBS was aspirated and 1 ml of homogenization buffer (320 mM sucrose, 4 mM HEPES NaOH, pH 7.4) supplemented with cOmplete EDTA-free protease inhibitor (Roche) and 1 mM ATP NaOH, pH 7.4. The cell pellet was uniformly resuspended with a 1 ml large bore tip (Fisher Scientific) and transferred to a 2 mL homogenizer (VWR International). To generate synaptosomes, the cells were homogenized with 25 steady strokes, with care taken to minimize formation of air bubbles. The homogenate was centrifuged at 2400g for 40 seconds to pellet unbroken cells. The supernatant was then transferred to a new tube and centrifuged at 14000g for 3 minutes to pellet synaptosomes. The supernatant was carefully removed and the pellet resuspended in 100 µl of homogenization buffer using a 200 ul large bore tip (Fisher Scientific). 900 µl of ice cold ddH_2O (MS grade) was added, and the liquid was immediately transferred to a 2 mL homogenizer. To lyse synaptosomes, the cells were homogenized with 12 steady strokes. Osmolarity was restored following homogenization by the addition of ATP, HEPES NaOH and cOmplete EDTA-free protease inhibitor to the same concentrations as in the homogenization buffer. Finally, the homogenate was centrifuged at 17000g for 3 minutes to remove any unbroken synaptosomes and debris. This process takes a total of ~12 minutes.

To immunoisolate SVs, 150 µl of suspended, prewashed magnetic HA beads (Thermo Fisher Scientific) were added to the supernatant and incubated at 4°C with end-over-end rotation for 15 minutes. For washes, beads were captured with a DynaMag Spin Magnet (Thermo Fisher Scientific) for 40 seconds. Four washes were performed in succession by the addition of 1 ml of KPBS (136 mM KCl, 10 mM KH2PO4, pH 7.25 in MS grade water) (Chen et al., 2016). Following the final wash, 25% of the KPBS-bead suspension was aliquoted for immunoblot analysis and the remaining 75% was subjected to metabolite extraction with 100 µl of 80% methanol/20% water supplemented with 500 µM internal amino acid standards. To ensure complete extraction, the beads were incubated with extraction mix for at least 10 minutes on dry ice prior to being separated from the mix. Extracted metabolites were subjected to a final 17000g spin for 3 minutes to remove any particulates and stored at -80°C until the MS run.

Immunoblotting – Protein from lysates were denatured by the addition of 50 µl of sample buffer. For whole cell lysates, 0.5 µl of Benzonase (EMD Millipore) was added and incubated with the lysates for at least 5 minutes to break down genomic DNA. Samples were resolved by 8%–16% SDS-PAGE, transferred for 2 hrs at room temperature at 45 V to 0.45 mm PVDF membranes, and analyzed by

immunoblotting as described previously (Chantranupong et al., 2016). Briefly, membranes were blocked with 5% milk prepared in TBST (Tris-buffered Saline with Tween 20) for at least 5 min at room temperature, then incubated with primary antibodies in 5% BSA TBST overnight at 4°C with end-over-end rotation. Primary antibodies targeting the following proteins were used at the indicated dilutions and obtained from the denoted companies: synaptophysin 1:2000 (SySy Cat # 101002), SV2A 1:2000 (SySy # 119003), HA 1:1000 (CST #C29F4), NMDAR 1:1000 (SySy #114011) (1:1000), synaptobrevin 1:5000 (SySy #104211), calreticulin 1:300 (CST #12238), VDAC 1:200 (CST#4661), LC3B 1:300 (CST #2775), GAPDH 1:2000 (CST #2118), synaptotagmin 1:1000 (SySy #105011), VGLUT1 1:2000 (SySy #135303), and VGLUT2 1:500 (SySy #135421) . Following overnight incubation, membranes were washed three times, 5 min each, with TBST and incubated with the corresponding secondary antibodies in 5% milk (1:5000) for 1 hour at room temperature. Membranes were then washed three more times, 5 min each, with TBST before being visualized using enhanced chemiluminescence (Thermo Fisher Scientific).

Endogenous tagging of synaptophysin – An endogenous triple HA tag was appended onto the C-terminus of synaptophysin using the vSLENDR method (Nishiyama et al., 2017). An AAV construct (below) containing a guide targeting the C-terminus of synaptophysin (underlined text), gRNA scaffold (bold italic text), 5' and 3' homology arms flanking this region (normal text), and the triple HA tag (gray highlighted text) replaced the mEGFP-cmak2a HDR cassette in the backbone of the pAAV-HDR-mEGFP-camk2a (Addgene #104589). This construct, which we term pAAV-HDR-sphys-3XHA, along with pAAV-EFS-SpCas9 were packaged at Boston Children's Viral Core. Cortical neurons cultured on a cover slip were coinfected on DIV3 with $3.45e^{7}$ genome copies (GC) of AAV-EFS-SpCas9 and $1.42e^{10}$ GC of AAV-HDR-sphys-3XHA. Neurons were processed for immunostaining at DIV12-14.

5' TTCTCCAATCAGATGTAATC***GTTTTAGAGCTAGAAATAGCAAGTTAAAATAAGGCTAGTCCGTTATCAACTTG AAAAAGTGGCACCGAGTCGGTGCTTTTTTGAATTC***TTTTGGTTTTGTTTGAGACAGGATCTACTTATGTGACCCT GGCTGTCCTGGAACTCACTACTCAGACCAGACTGGCCTCAAACTCACAGACCTCTGCTTGCCTCTGCCTCCTGA GTACTAAGATGAAGACTGCACCACCACACCCAGCCCAAAAATGAGTTGTTTGAGGCTGACTTTCATGTTGCACAG GCTAGCCTCAAACTATGAATTTAAAGGTAGACTTGAATTTCTGGGTAGTGGAGGCAGAGACAGGCGACTTCTATG AGTTCCAGGCCAGCCTGGTCTACAGAGTGAATTCCAGGACAGCCAGGGCTGCAGAGAGACCCTGTCTCAAAAA AAAAAAGCTAGCCTTGAAGTGATCGCCCCTGCCTCCAGCTTCCTAAGATTACAAGATGTGGGCCTTCAGACTTGT CCATGTAAACACTGATAGAAGTTGAACATCATGGGAATCTAACACACACACACACACTCCCAAGTTTTTCTGTACA CTGATAGTCATAGAGGCCCACGAATTTATGCCCTAAAAATGCCCATTCCTGTTCACTCAGCCTCAAAGACCCTGG GGCTGCCGAGGCAATGGGTAAGAGACAACAGCTTTGGTCATGTCTCCCTGCAGGTGTTTGGCTTCCTGAACCTG GTGCTCTGGGTTGGCAACCTATGGTTCGTGTTCAAGGAGACAGGCTGGGCCGCCCCATTCATGCGCGCACCTC CAGGCGCCCCAGAAAAGCAACCAGCTCCTGGCGATGCCTACGGCGATGCGGGCTATGGGCAGGGCCCCGGAG GCTATGGGCCCCAGGACTCCTACGGGCCTCAGGGTGGTTATCAACCCGATTACGGGCAGCCAGCCAGCGGCG GTGGCGGTGGCTACGGGCCTCAGGGCGACTATGGGCAGCAAGGCTACGGCCAACAGGGTGCGCCCACCTCCT TCTCCAACCAAATGGGAGGGAGCGGCTATCCCTATGACGTGCCTGATTACGCCGGCACAGGATCCTACCCCTAT GATGTGCCTGACTACGCTGGCAGCGCCGGATACCCTTATGATGTGCCTGATTATGCTTAATCTGGTGAGTGACA

ACTGGGCGGATGCGGTAGGCAGGGAGCATACAAGGAGTGAAGTTTGAAGGAACCAATAGATAGGCAGAACCAA
AAAAAAAAAAAGGTGAACTTGGTAAAACTAGCCAATGAGAGGAACCGTGAGAAGGAAGGGGACGGAGCAGTGC
TCAGAGTAACCAATGAAAGGAGTGTAGGGGCACTTGCGCAGTGGAGAATCACCAAAGTGGTGTAGGTTTCCAGG
AAGGGAAGGGGAGGAGGGTCTTTGAAATCATTGGTAAACCAATAGGCGGTAACGCCAGTAGGTGGAAGAAGGT
AAACACGTTGGGTTTTGAAGGGCGCTAGCGCTAAAGCAGGATGTAGGTCAGCTGCTACCTCTCCTTAACCCTTT
AATGAAAGAGAGAGTTTGGAATTTCAAATGAGGAAAAGGGGAGGGCTGGAGGCCTTAGAAACACGAGTATGCCT
TTTTGTTGGGCCTTTAAAAAATGAATGCCGCCGGACGGTGGAGGCGCACGCCTTTAATCCCAGCACTTGGGAGG
CAGAAGCAGGCGGAGTTTTTGAGTTCGAGGCCAGCCTGGTCTACAAAGTGAGTTCCAGGACAGCCAGGGCTAT
ACAGAGAAACCCTGTCGCGAAAAAAAAAAAAAAAAAAAAACCCTGCCTGGTGTGATGGAGCACATATATAATCCC
AGCACTTGAGAGGTAGAGGCATGGGGATTGCAAGTTCTCGAGTCCTGCGTGGTCAGTATAGCCCAATCCTGTCT
TAAACAGAGACGGTAACAGCATCTAGGTGGGAGCAGATGTGGTCCTGGGTGAGCCTTCTACAGCAACCCACATT
TAATTGTTTTTAAACTCCTTGGACAGGCTCTGAGACACACCTTTAAGCACAGCTCTGGGGGAATTAGAGACAGGC
CTAGGTCTCTTGTTTTGCAAAGCAATTTCCAGGCTGC 3’

Immunohistochemistry – Cells were fixed in 4% PFA 4% sucrose in PBS for 10 minutes, and washed in PBS twice for 10 minutes each with shaking at room temperature. Cells were then blocked in 1 ml of blocking solution (10% BSA, 10% normal goat serum, PBS) for 30 minutes at room temperature. Cells were washed with 1 ml of TBST (0.2% TritonX-100 in PBS) for 10 minutes. Primary antibodies were suspended in BTBST (1% BSA, 1% normal goat serum PBS) and 300 ul was added to each slip. The following concentrations were used: synapsin 1:500 (CST #5297), synaptophysin 1:1000 (SySy 101004), synaptotagmin 1:1000, and HA 1:500 (CST#2367). Cells were incubated overnight at 4°C or at room temperature for 1.5 hours. Following this, cells were washed three times, 10 minutes each, in 1 ml of PBS with rocking at room temperature. The following secondary antibodies (Thermo Fisher Scientific) were diluted in BTBST and added at a 1:500 dilution: goat anti-rabbit Alexa Fluor 488, goat anti-guinea pig Alexa Fluor 488, goat anti-rabbit Alexa Fluor 647. Cells were covered from light and incubated at room temperature for 2 hours, washed 3 more times in PBS for 10 minutes each and mounted on cover slides with Floromount G (Thermo Fisher Scientific). Slips were imaged an Olympus VS120 slide scanning microscope.

Transmission Electron Microscopy – To free SVs from beads, we relied on a protease strategy as the HA binding strength to its cognate antibody is too strong to be dissociated by peptide competition. We used ficin (Sigma), a cysteine protease that can rapidly digest murine monoclonal IgGs (Mariani et al., 1991). Following the IP, SVs were equilibrated with three washes of ficin buffer (50 mM Tris pH 7.0, 2 mM EDTA, 1 mM cysteine). The supernatant was removed and replaced with 100 µl of ficin buffer supplemented with 5 mg/ml ficin (Sigma). SVs were incubated at 37°C for 20 minutes to enable ficin to be active. Supernatant was removed and immediately chilled on ice prior to EM analysis. Images were acquired at the Electron Microscopy Core at Harvard Medical School. 5µl of the sample was adsorbed for 1 minute to a carbon coated grid that had been made hydrophilic by a 30 second exposure to a glow discharge. Excess liquid was removed with a filter paper (Whatman #1) and the samples were stained

with 0.75% uranyl formate for 30 seconds. After removing the excess uranyl formate with a filter paper the grids were examined in a JEOL 1200EX Transmission electron microscope or a TecnaiG² Spirit BioTWIN and images were recorded with an AMT 2k CCD camera.

Luminescence Assay for Glutamate – Following immunoisolation, SVs were permeabilized with 70 µl of Triton elution buffer (1% TritonX-100, 500 mM NaCl, 5 mM HEPES pH 7.4) and incubated at 37°C for 20 minutes to ensure complete permeabilization. 15 l of this eluent was saved for immunoblot analyses. To detect glutamate, the Glutamate Glo Assay Kit (Promega) was used. 50 µl of eluent was combined into a 96 well plate with a 50 µl mix of Luciferin detection solution, which contains reductase, reductase substrate, glutamate hydrogenase, and NAD as specified. The mixture was incubated at room temperature for 1 hr and luminescence was detected with a florescent plate reader (BioTek).

Proteomics run and analysis – To ensure sufficient yields for proteomic analysis, each sample combined cells from three plates, for a total of 15 million neurons. Following immunoisolation, SVs were permeabilized with 70 µl of Triton elution buffer at 32°C for 20 minutes. Eluents from the three plates were pooled into a common tube. 20 µl of this mix was saved for immunoblot analysis. The remaining eluent was transferred to a new tube and subjected to TCA precipitation. Briefly, the volume of eluent was raised to 400 µl with MS grade, ice cold water. 100 µl of 100% tricloroacetic acid (TCA) was added to this mixture.

Precipitated proteins were submitted to the Taplin Mass Spectrometry Core for proteomic analysis. There, samples were digested with 50 µl of 50 mM ammonium bicarbonate solution containing 5 ng/µl modified sequencing-grade trypsin (Promega, Madison, WI) at 4°C. After 45 min., the excess trypsin solution was removed and replaced with 50 mM ammonium bicarbonate solution to just cover the gel pieces. Samples were then placed in a 37°C room overnight. Peptides were later extracted by removing the ammonium bicarbonate solution, followed by one wash with a solution containing 50% acetonitrile and 1% formic acid. The extracts were then dried in a speed-vac (~1 hr). The samples were then stored at 4°C until analysis.

On the day of analysis the samples were reconstituted in 5 - 10 µl of HPLC solvent A (2.5% acetonitrile, 0.1% formic acid). A nano-scale reverse-phase HPLC capillary column was created by packing 2.6 µm C18 spherical silica beads into a fused silica capillary (100 µm inner diameter x ~30 cm length) with a flame-drawn tip (Peng and Gygi, 2001). After equilibrating the column each sample was loaded via a Famos auto sampler (LC Packings, San Francisco CA) onto the column. A gradient was formed and peptides were eluted with increasing concentrations of solvent B (97.5% acetonitrile, 0.1% formic acid).

As peptides eluted they were subjected to electrospray ionization and then entered into an LTQ Orbitrap Velos Pro ion-trap mass spectrometer (Thermo Fisher Scientific, Waltham, MA). Peptides were detected, isolated, and fragmented to produce a tandem mass spectrum of specific fragment ions for

each peptide. Peptide sequences (and hence protein identity) were determined by matching protein databases with the acquired fragmentation pattern by the software program, Sequest (Thermo Fisher Scientific, Waltham, MA) (Eng et al., 1994). All databases include a reversed version of all the sequences and the data was filtered to between a one and two percent peptide false discovery rate.

Mice – The following mouse strains/lines were used in this study: CD-1® IGS (Charles River Laboratories, Stock # 022); C57BL/6J (The Jackson Laboratory, Stock # 000664); DAT-IRES-Cre (The Jackson Laboratory, Stock #006660)(referred to as *Slc6a3*$^{IRES\text{-}Cre}$ mice); VGAT-IRES-Cre (The Jackson Laboratory, Stock #016962) (referred to as *Slc32a1*$^{IRES\text{-}Cre}$ mice); genetically targeted *Adora2a*-Cre BAC transgenic mice (GENSAT, founder line KG139), which express Cre under transcriptional control of the adenosine A2A receptor genomic promoter (Durieux et al., 2009). All animals were kept on a regular 12:12 light/dark cycle under standard housing conditions. All experimental manipulations were performed in accordance with protocols approved by the Harvard Standing Committee on Animal Care following guidelines described in the US National Institutes of Health Guide for the Care and Use of Laboratory Animals.

SV isolation from whole brain – Mice were rapidly anesthetized with isoflurane and brains were quickly extracted from mice on ice. To ensure more efficient homogenization, each brain was divided in half along the midline and transferred immediately to a homogenizer containing 1.5 mls of ice-cold lysis buffer (KPBS supplemented with 1 mM ATP and cOmplete EDTA-free protease inhibitor). Brains were rapidly lysed with 30 strokes using a motorized homogenizer, taking care not to introduce bubbles. Lysates were transferred to prechilled 2 ml tubes and centrifuged at 17000 g for 3 minutes to pellet unbroken cells, contaminating organelles and debris. Supernatants were transferred to new 1.5 ml tubes and subjected to IP with 150 ul HA beads for 15 minutes with end-over-end rotation. Following the IP, the beads were washed 4 times in KPBS supplemented with 500 mM NaCl to enhance cleanliness. In the final wash, the IP was incubated with end-over-end rotation at 4°C for 5 minutes to further remove contaminants. Following this final wash, immunoprecipitates were processed for immunoblot and metabolite analysis as described for cortical culture SVs described above.

Stereotaxic injections – Injections were performed as previously described (Huang et al., 2019). AAVs for SV-Tag was obtained from Boston Children's Virus Core and infused at a concetration of ~10^12 GC/ml. AAVs were infused into target regions at approximately 50 nl/min using a syringe pump (Harvard Apparatus, #883015), and pipettes were slowly withdrawn (<10 µm/s) at least 8 min after the end of the infusion. All coordinates are relative to Bregma along the anterior-posterior (AP) axis and medial-lateral (ML) axis, and relative to the pial surface along the dorsoventral axis (DV). Coordinates for injections are as follows: cortex site 1: AP = -2.5 mm, ML = -2.0 mm, DV = −0.4 mm, cortex site 2: AP = -1.0 mm, ML = -1.5 mm, DV = −0.4 mm , striatum: AP = +0.6 mm, ML = 1.7 mm, DV = −3.33 mm, hippocampus AP

= -2.5 mm, ML = -1.5 mm, DV = −1.5 mm; hippocampus transverse (for paired pulse ratio measurements): AP = -2.9 mm, ML = -3.15 mm, DV = −3.3 mm, substantia nigra: AP = -3.3 mm, ML = -1.5 mm, DV = −4.3 mm. Bilateral injections were performed for all mice used, with the exception of cortex, in which 4 injections were performed to maximally cover the cortical area. Following wound closure, mice were placed in a cage with a heating pad until their activity was recovered before returning to their home cage. Mice were given pre- and post-operative oral carprofen (MediGel CPF, 5 mg/kg/day) as an analgesic, and monitored daily for at least 4 days post-surgery.

Immunohistochemistry – Mice were anaesthetized by isoflurane inhalation and perfused cardiacly with PBS followed by 4% PFA in PBS. Brains were extracted and stored in 4% PFA PBS for at least 8 hours. Brains were sliced into 70 μm thick free-floating sections with a Leica VT1000 s vibratome. Selected slices were transferred to a clean 6 well plate and rinsed three times, 5 minutes each in PBS. They were then blocked with rotation at room temperature for an hour in blocking buffer (5% normal goat serum (Abcam), 0.2% TritonX-100 PBS). Blocking buffer was removed and replaced with 500 μl of a solution containing a 1:500 dilution of anti- tyrosine hydroxylase antibody (Millipore Sigma). Slices were incubated overnight with side to side rotation at 4°C. The next day, slices were transferred to a clean well and washed 5 times, 5 minutes each in PBST (PBS with 0.2% TritonX-100). Following the final wash, slices were incubated for 1.5 hours in 500 μl of secondary antibody (goat anti mouse Alexa Fluor 647) diluted 1:500 in blocking buffer. Slices were washed four times in PBST, then four times in PBS for 5 minutes (5 minutes for each wash) before mounting with Floromount G (Thermo Fisher Scientific). Slices were imaged an Olympus VS120 slide scanning microscope, including those housed in the Neuro Imaging Facility.

Electrophysiology – Coverslips containing cultured neurons or acute brain slices were transferred into a recording chamber mounted on an upright microscope (Olympus BX51WI) and continuously superfused (2–3 ml min^{-1}) with ACSF containing (in mM) 125 NaCl, 2.5 KCl, 25 $NaHCO_3$, 2 $CaCl_2$, 1 $MgCl_2$, 1.25 NaH_2PO_4 and 25 glucose (295 mOsm kg^{-1}). ACSF was warmed to 32–34 °C by passing it through a feedback-controlled in-line heater (SH-27B; Warner Instruments). Cells were visualized through a 60X water-immersion objective with either infrared differential interference contrast optics or epifluorescence to identify tdTomato$^+$ cells. For whole cell voltage clamp recordings, patch pipettes (2–4 MΩ) pulled from borosilicate glass (G150F-3, Warner Instruments) were filled with a Cs^+-based low Cl^- internal solution containing (in mM) 135 $CsMeSO_3$, 10 HEPES, 1 EGTA, 3.3 QX-314 (Cl^- salt), 4 Mg-ATP, 0.3 Na-GTP, 8 Na_2-phosphocreatine (pH 7.3 adjusted with CsOH; 295 mOsm·kg^{-1}) For voltage clamp recordings, mEPSCs were recorded for 5 min in the presence of 1 μM tetrodotoxin (Tocris), 10 μM CPP (Tocris), and 10 μM gabazine (Tocris) at a holding potential of -70 mV. Paired evoked EPSCs for probability of release measurements were recorded as previously described (Jackman et al., 2016). Briefly, a cut was made between CA3 and CA1 to prevent recurrent excitation. Extracellular stimulation was performed with a

652 stimulus isolation unit (Iso-flex). Bipolar electrodes (PlasticOne) were placed near CA3 proximal to the cut
653 and stimulation parameters were 20 Hz, 50-100uA. Paired evoked-EPSCs from CA1 cells were recorded
654 at a holding potential of -70mV with 10μM gabazine added to the bath.
655
656 **Acute brain slice preparation** – Brain slices were obtained from 2-4-month-old mice (both male and
657 female) using standard techniques. Mice were anaesthetized by isoflurane inhalation and perfused
658 cardiacly with ice-cold ACSF containing (in mM) 125 NaCl, 2.5 KCl, 25 $NaHCO_3$, 2 $CaCl_2$, 1 $MgCl_2$, 1.25
659 NaH_2PO_4 and 25 glucose (295 mOsm kg^{-1}). Brains were blocked and transferred into a slicing chamber
660 containing ice-cold ACSF. Coronal slices of striatum for amperometric recordings or transverse slices of
661 hippocampus (for probability of release measurements) were cut at 300 μm thickness with a Leica
662 VT1000 s vibratome in ice-cold ACSF, transferred for 10 min to a holding chamber containing choline-
663 based solution (consisting of (in mM): 110 choline chloride, 25 $NaHCO_3$, 2.5 KCl, 7 $MgCl_2$, 0.5 $CaCl_2$, 1.25
664 NaH_2PO_4, 25 glucose, 11.6 ascorbic acid, and 3.1 pyruvic acid) at 34°C then transferred to a secondary
665 holding chamber containing ACSF at 34C for 10 min and subsequently maintained at room temperature
666 (20–22°C) until use. All recordings were obtained within 4 hr of slicing. Both choline solution and ACSF
667 were constantly bubbled with 95% O_2/5% CO_2.

668 **Amperometric recordings** – To deplete presynaptic terminals of dopamine, *Slc6a3*$^{IRES-Cre}$ mice were
669 administered the VMAT2 antagonist tetrabenazine (Sigma, 30 mg kg^{-1} intraperitoneally) 2 h before slicing.
670 Control mice were injected with a DMSO/Saline mixture containing the same proportion of both solvents
671 as would be used for a tetrabenazine injection. Constant-potential amperometry was performed as
672 previously described (Tritsch et al., 2012). Briefly, glass-encased carbon-fiber microelectrodes (CFE1011
673 from Kation scientific - 7 μm diameter, 100 μm length) were placed approximately 50-100 μm within dorsal
674 striatum slices and held at a constant voltage of + 600 mV versus Ag/AgCl by a Multiclamp 700B amplifier
675 (Molecular Devices). Electrodes were calibrated with fresh 5 μM dopamine standards in ACSF to
676 determine CFE sensitivity and to allow conversion of current amplitude to extracellular dopamine
677 concentration. Dopaminergic terminals surrounding the CFE were stimulated by Bipolar electrodes with
678 0.1 ms and 100-250 μA delivered at 3 min intervals.

679 **Data acquisition and analysis** – Membrane currents were amplified and low-pass filtered at 3 kHz using
680 a Multiclamp 700B amplifier (Molecular Devices), digitized at 10 kHz and acquired using National
681 Instruments acquisition boards and a custom software (https://github.com/bernardosabatini/SabalabAcq)
682 written in MATLAB (Mathworks). Amperometry and electrophysiology were analyzed offline using Igor Pro
683 (Wavemetrics). Detection threshold for mEPSCs was set at 7 pA. Averaged waveforms were used to
684 obtain current latency, peak amplitude, 10–90% rise time and decay time. Current onset was measured
685 using a threshold set at three standard deviations of baseline noise. Peak amplitudes were calculated by
686 averaging over a 2 ms window around the peak. Data were compared statistically by unpaired two-tailed
687 Student's t-test. *P* values less than 0.05 were considered statistically significant.

GC/MS – GC-MS analysis was carried out and analyzed as described (Parker et al., 2017). In brief, dried, extracted metabolites were derivatized using a MOX-tBDMCS method and analyzed by GC-MS using a DB-35MS column (30m x 0.25mm i.d., 0.25µm) in an Agilent 7890B gas chromatograph interfaced with a 5977B mass spectrometer. Metabolites were identified by unique fragments and retention time in comparison to known standards. Peaks were picked in OpenChrom and integrated and corrected for natural isotopic abundance using in-house algorithms adapted from Fernandez et al (Fernandez et al., 1996; Lewis et al., 2014; Wenig and Odermatt, 2010).

LC-MS/MS with the hybrid metabolomics method – Samples were subjected to an LCMS analysis to detect and quantify known peaks. A metabolite extraction was carried out on each sample with a previously described method (Pacold et al., 2016). The LC column was a Millipore™ ZIC-pHILIC (2.1 x150 mm, 5 µm) coupled to a Dionex Ultimate 3000™ system and the column oven temperature was set to 25^{O}C for the gradient elution. A flow rate of 100 µL/min was used with the following buffers; A) 10 mM ammonium carbonate in water, pH 9.0, and B) neat acetonitrile. The gradient profile was as follows; 80-20%B (0-30 min), 20-80%B (30-31 min), 80-80%B (31-42 min). Injection volume was set to 1 µL for all analyses (42 min total run time per injection). MS analyses were carried out by coupling the LC system to a Thermo Q Exactive HF™ mass spectrometer operating in heated electrospray ionization mode (HESI). Method duration was 30 min with a polarity switching data-dependent Top 5 method for both positive and negative modes. Spray voltage for both positive and negative modes was 3.5kV and capillary temperature was set to 320^{O}C with a sheath gas rate of 35, aux gas of 10, and max spray current of 100 µA. The full MS scan for both polarities utilized 120,000 resolution with an AGC target of 3e6 and a maximum IT of 100 ms, and the scan range was from 67-1000 *m*/*z*. Tandem MS spectra for both positive and negative mode used a resolution of 15,000, AGC target of 1e5, maximum IT of 50 ms, isolation window of 0.4 m/z, isolation offset of 0.1 m/z, fixed first mass of 50 m/z, and 3- way multiplexed normalized collision energies (nCE) of 10, 35, 80. The minimum AGC target was 1e4 with an intensity threshold of 2e5. All data were acquired in profile mode.

Metabolomics Data Processing

Relative quantification of metabolites – The resulting Thermo™ RAW files were converted to mzXML format using ReAdW.exe version 4.3.1 to enable peak detection and quantification. The centroided data were searched using an in-house python script Mighty_skeleton version 0.0.2 and peak heights were extracted from the mzXML files based on a previously established library of metabolite retention times and accurate masses adapted from the Whitehead Institute (Chen et al., 2016), and verified with authentic standards and/or high resolution MS/MS spectral manually curated against the NIST14MS/MS (Voge et al., 2016) and METLIN (2017) (Smith et al., 2005) tandem mass spectral libraries. Metabolite peaks were extracted based on the theoretical *m*/*z* of the expected ion type e.g., $[M+H]^+$, with a ±5 part-

per-million (ppm) tolerance, and a ± 7.5 second peak apex retention time tolerance within an initial retention time search window of ± 0.5 min across the study samples.

Detection of untargeted features – The MS1 level data in both positive and negative mode were searched for representative features across all study files using an in-house python script called Ungrid (version 0.5). The algorithm reduces all detected MS1 peak data into representative features by sorting intensity from high to low (across all samples) and then applying an array bisection algorithm (python v3.0.1) on the m/z and retention time values with custom tolerances (25 ppm m/z tolerance for peak discrimination, 0.5 min RT delta for chromatographic discrimination, 1e5 minimum intensity, 10X signal to noise (within spectrum)). The output is a list of representative high intensity features of a defined m/z and retention time. These feature intensities were then extracted across all samples using Mighty_skeleton (above) to give the peak intensities for each feature in each sample.

Metabolomics informatics – The resulting data matrices of metabolite intensities for all samples and blank controls (either retention time library data or untargeted data) was processed with an in-house statistical pipeline Metabolyze version 1.0 and final peak detection was calculated based on a signal to noise ratio (S/N) of 3X compared to blank controls, with a floor of 10,000 (arbitrary units). For samples where the peak intensity was lower than the blank threshold, metabolites were annotated as not detected, and the threshold value was imputed for any statistical comparisons to enable an estimate of the fold change as applicable. The resulting blank corrected data matrix was then used for all group-wise comparisons, and t-tests were performed with the Python SciPy (1.1.0) (Jones E, et al) library to test for differences and generate statistics for downstream analyses. Any metabolite with p-value < 0.05 was considered significantly regulated (up or down). Any outliers were omitted with the Grubb's outlier test. Values are reported as log2 fold changes ± standard error of the mean. In order to adjust for significant covariate effects (as applicable) in the experimental design the R package, DESeq2 (1.24.0) (Love et al., 2014) was used to test for significant differences. Data processing for this correction required the blank corrected matrix to be imputed with zeroes for non-detected values instead of the blank threshold to avoid false positives. This corrected matrix was then analyzed utilizing DESeq2 to calculate the adjusted p-value in the covariate model.

Targeted LC/MS for dopamine detection – Metabolite profiling was conducted on a QExactive bench top orbitrap mass spectrometer equipped with an Ion Max source and a HESI II probe, which was coupled to a Dionex UltiMate 3000 HPLC system (Thermo Fisher Scientific, San Jose, CA). External mass calibration was performed using the standard calibration mixture every 7 days. 5 µL were injected onto a SeQuant® ZIC®-pHILIC 150 x 2.1 mm analytical column equipped with a 2.1 x 20 mm guard column (both 5 mm particle size; EMD Millipore). The following method was adapted from Tufi et al. (2015): Buffer A was 10 mM ammonium formate with 0.2% formic acid in 90% acetonitrile; Buffer B was water with 0.2% formic acid. The column oven and autosampler tray were held at 25◦C and 4◦C,

758 respectively. The chromatographic gradient was run at a flow rate of 0.300 mL/min as follows: 0-2 min:
759 hold at 0% B; 2.5-15 min.: linear gradient form 0-40% B; 15.5-16 min.: linear gradient from 40-0% B; 16-
760 21 min.: hold at 0% B. The mass spectrometer was operated in full-scan, polarity-switching mode, with
761 the spray voltage set to 3.0 kV, the heated capillary held at 275◦C, and the HESI probe held at 350◦C. The
762 sheath gas flow was set to 40 units, the auxiliary gas flow was set to 15 units, and the sweep gas flow
763 was set to 1 unit. MS data acquisition was performed in a range of *m/z* =70-1000, with the resolution set
764 at 70,000, the AGC targeted at $1x10^6$, and the maximum injection time was 20 msec. In addition, timed
765 targeted selected ion monitoring (tSIM) scans were included in positive mode to enhance detection of
766 Dopamine (*m/z* 154.08626). MS settings were as described above, with the AGC target set at $1x10^5$, the
767 maximum injection time was 200 msec, and the isolation window was 1.0 *m/z*.
768
769 **Acknowledgements**
770
771 We thank all members of the Sabatini lab for helpful suggestions and advice, in particular T.
772 Consedine and G. Radeljic for technical assistance and K. Mastro, S. Melzer, and A. Girasole for
773 manuscript input. We also thank W.W. Chen, M.A. Remaileh, and D.S. Koda for insightful input in
774 methodology and/or data analysis. We thank the Electron Microscopy Core at Harvard Medical School for
775 generous assistance with the EM imaging, C.A. Lewis at the Whitehead Metabolite Profiling Core Facility
776 for the MS runs and analysis of dopamine, and the Taplin Mass Spectrometry Core for proteomic runs
777 and analysis. This work was supported by grants from the Howard Hughes Medical Institute and
778 R37NS046579 from NINDS to B.L.S.; the Hanna Gray Fellowship from the Howard Hughes Medical
779 Institute to L.C.; the Mary Kay Foundation (Cancer Research Grant 017-032), the Shifrin-Myers Breast
780 Cancer Discovery Fund at NYULMC, a V Foundation V Scholar Grant funded by the Hearst Foundation
781 (V2017-004), and an NCI K22 Career Transition Award (1K22CA212059) to M.E.P.; (NIH) R01
782 NS108151-01, (FNIH) RFA 2018-PACT001, and (NIH) HHS-NIH-NIAD-BAA2018 to D.R.J.; and NINDS
783 P30 Core Center Grant #NS072030 to the Neuro Imaging Facility.
784
785 **Declaration of Interests**
786
787 The authors declare no competing interests

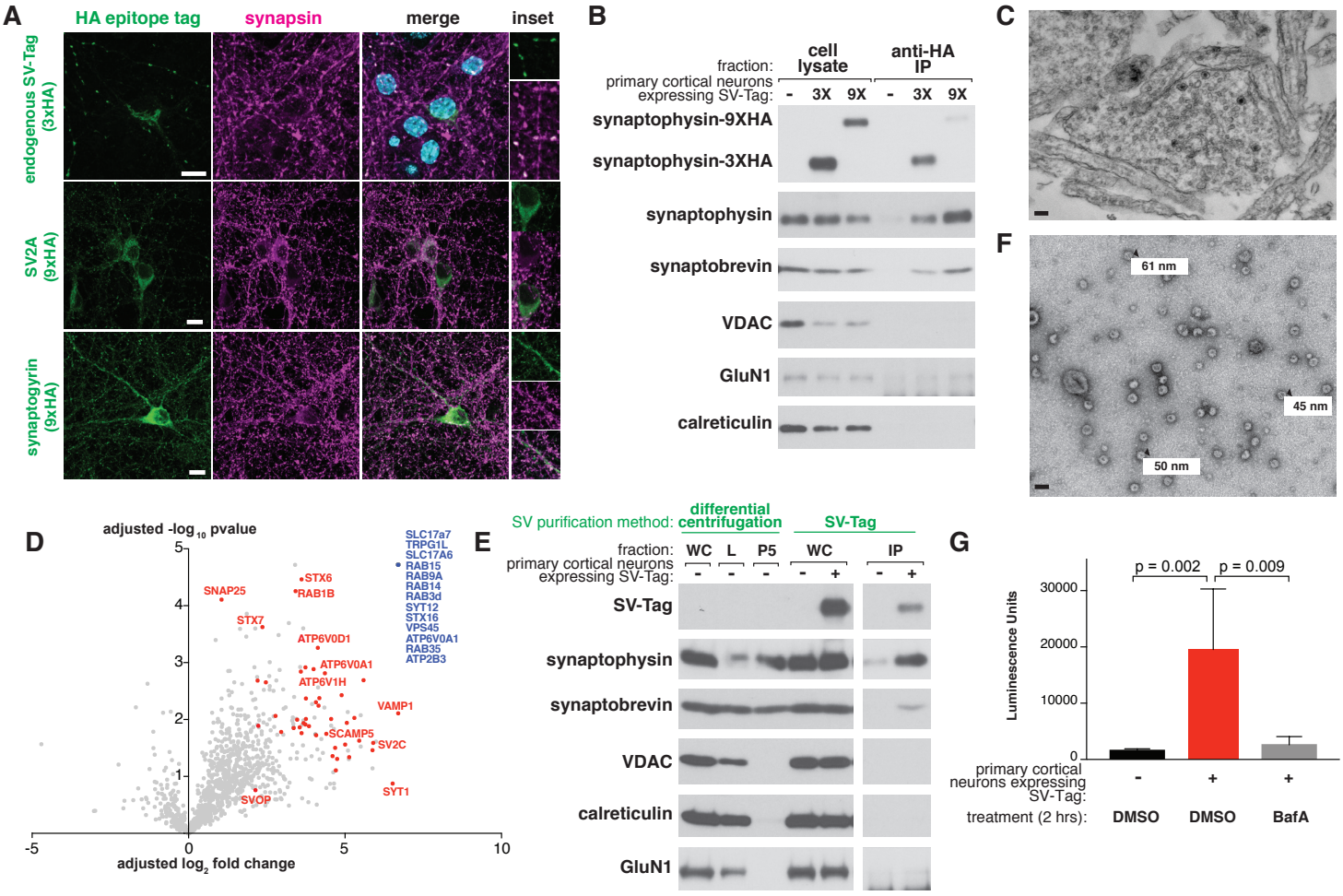

Supplemental Figure 1:

(**A**) Immunostaining of primary neurons expressing indicated HA-tagged proteins (green) and endogenous synapsin (magenta). Specifically, neurons are expressing endogenously tagged synaptophysin with a triple HA tag (top row), SV2A tagged at the N terminus with nine HA tags (9x HA) (middle row), and synaptogyrin tagged at the N terminus with a 9X HA tag (bottom row). Insets represent selected fields that were magnified 1.7X (top row) and 1.35X (middle and bottom row). Scale bars, 10 μm. (**B**) Immunoblot analysis of the effect of the number of HA tags on the efficiency of SV isolation. Lysates were prepared from neurons infected with lentivirus encoding for synaptophysin conjugated to three HA tags (3X) or nine HA tags (9X). (**C**) Electron microscope image of synaptosomes generated with the workflow. Scale bar, 100 nm (**D**) Proteomics analysis of isolated SVs versus control IP. The blue dot denotes proteins in which there were no detected peptides in the control IP (n = 70, 14 of which are validated synaptic vesicle proteins), and red dots represent established synaptic vesicle proteins based on literature. (**E**) Immunoblot analysis of SVs isolated with the SV-Tag based workflow compared to a previously established one based on differential centrifugation. WC: whole cell, L: whole cell lysate, P5: synaptic vesicle pellet, IP: HA immunoprecipitate (**F**) Electron microscope image of SVs generated with the differential centrifugation method used in S1E. Values denote diameter of indicated particles. Scale bar, 100 nm (**G**) Luminescence-based detection of glutamate in SVs isolated from neurons treated with DMSO or Bafilomycin A (500 nM) 2 hours prior to isolation.

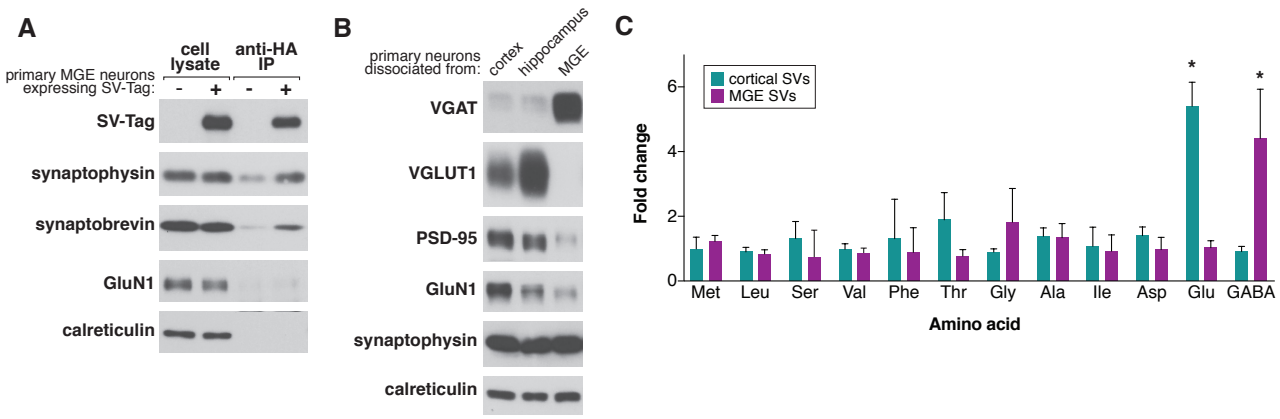

Supplemental Figure 2:

(**A**) Immunoblot analysis of indicated proteins in whole cell lysates, HA immunoprecipitates from medial ganglionic eminence (MGE) cultures infected with SV-Tag, and control immunoprecipitates from uninfected MGE cultures. (**B**) Immunoblot analysis of whole cell lysates of primary cortical, hippocampal, and MGE neurons. Lysates were probed for the presence of indicated synaptic and pan neuronal markers. (**C**) Comparison of the relative abundances of specified amino acids in purified synaptic vesicles isolated from cortical versus MGE cultures and profiled with GC/MS (mean ± SEM, n=3). Asterisk denotes statistical significance. Glutamate fold change p value = $7.5e^{-5}$, GABA fold change p value = $4.8e^{-3}$

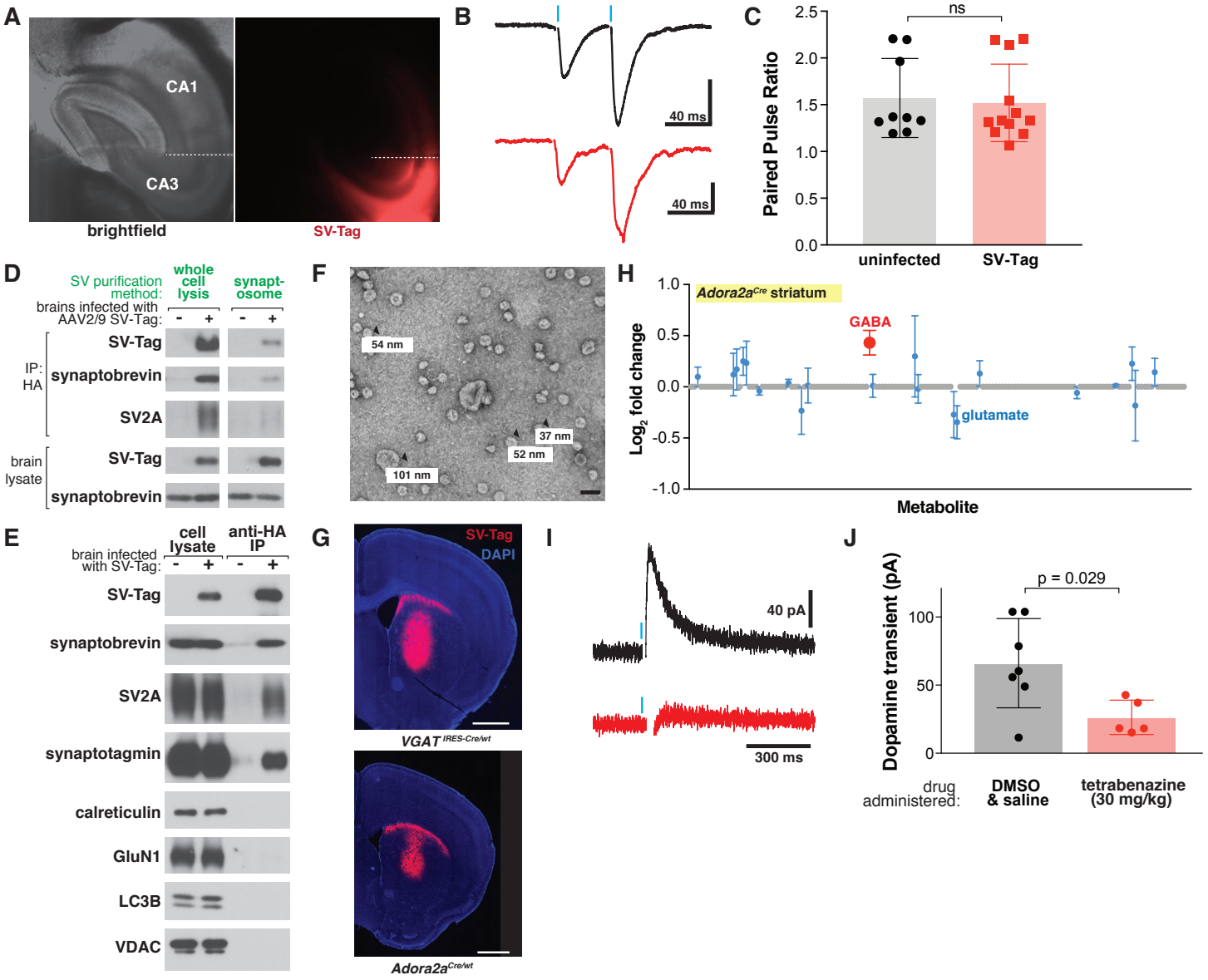

Supplemental Figure 4:

(**A**) Immunofluorescence images of transverse sections containing hippocampal CA3 transduced with synaptophysin-9XHA. A cut was made between CA2 and CA1 (dashed white line) to prevent recurrent excitation of these synapses. (**B**) Representative traces of evoked current responses in hippocampus from electrical stimulation. Vertical blue bars indicate stimulation that occurred with an interstimulus interval of 50 ms of Schaffer collaterals with (red) and without (black) expression of SV-Tag. Vertical bar indicates 100 pA. Non-significant p value = n.s. (**C**) Summary of paired pulse ratios of electrically evoked synaptic responses from CA3 to CA1 synapses that were uninfected or expressing SV-Tag. (**D**) Immmunoblot analysis of indicated proteins for synaptic vesicles isolated from the whole cell lysis method of brains compared to vesicles isolated with the synaptosome method. (**E**) Immunoblot analysis of synaptic vesicles isolated from mouse brains transduced with SV-Tag in the cortex. (**F**) Electron microscope image of synaptic vesicles generated with the workflow. Values denote diameter of indicated

particles. Scale bar: 100 nm (**G**) Coronal sections from *Slc32a1*$^{\text{IRES-Cre/wt}}$ (*VGAT*$^{\textit{IRES-Cre/wt}}$) and *Adora2a*$^{\textit{Cre/wt}}$ mice transduced with a Cre-dependent SV-Tag in the striatum. (**H**) LC/MS profile of synaptic vesicles isolated from *Adora2a*$^{\textit{Cre/wt}}$ mice brains infected with SV-Tag in striatum compared with uninfected brains. (mean ± SEM, n=4) (**I**) Representative traces of amperometry demonstrating the effects of DMSO (black) and tetrabenazine (black) on evoked dopamine. Blue indicates electrical stimulation. (**J**) Amperometry for dopamine in coronal slices prepared from mice administered intraperitoneally with tetrabenazine (30mg/kg) or vehicle control 2 hours before slicing.

Supplemental Table 1:
Proteomics profile of immunoprecipitates from primary cortical neurons expressing SV-Tag versus uninfected neurons, related to Figure S1D.

Supplemental Table 2:
List of the metabolites interrogated in the targeted LC/MS runs, related to Figure 2C, D and F, Figure 4D, E and G, and Figure S4H.

Supplemental Table 3:
Metabolites detected in SVs from cortical cultures via GC/MS and LC/MS and their associated calculations of fold changes, significance, and SEM, related to Figure 2.

Supplemental Table 4:
Metabolites detected via global LC/MS performed on cortical culture SVs, treated with DMSO or BafilomycinA, related to Figure 3.

Supplemental Table 5:
Metabolites detected in SVs from hippocampus and striatum via LC/MS and their associated calculations of fold changes, significance, and SEM, related to Figure 4.

References

Abu-Remaileh, M., Wyant, G.A., Kim, C., Laqtom, N.N., Abbasi, M., Chan, S.H., Freinkman, E., and Sabatini, D.M. (2017). Lysosomal metabolomics reveals V-ATPase- and mTOR-dependent mechanisms for the efflux of amino acids from lysosomes. Science (80-.). *358*, 4.

Ahmed, S., Holt, M., Riedel, D., and Jahn, R. (2013). Small-scale isolation of synaptic vesicles from mammalian brain. Nat. Protoc. *8*, 998–1009.

Atasoy, D., Aponte, Y., Su, H.H., and Sternson, S.M. (2008). A FLEX Switch Targets Channelrhodopsin-2 to Multiple Cell Types for Imaging and Long-Range Circuit Mapping. J. Neurosci. *28*, 7025–7030.

Beale, D.J., Pinu, F.R., Kouremenos, K.A., Poojary, M.M., Narayana, V.K., Boughton, B.A., Kanojia, K., Dayalan, S., Jones, O.A.H., and Dias, D.A. (2018). Review of recent developments in GC – MS approaches to metabolomics-based research (Springer US).

Beaudoin III, G.M.J., Lee, S., Singh, D., Yuan, Y., Ng, Y., Reichardt, L.F., and Arikkath, J. (2012). Culturing pyramidal neurons from the early postnatal mouse hippocampus and cortex. Nat. Protoc. *7*, 1741–1754.

Bowman, E.J., Sieberst, A., and Altendorft, K. (1988). Bafilomycins : A class of inhibitors of membrane ATPases from microorganisms , animal cells , and plant cells. *85*, 7972–7976.

Burger, P.M., Mehl, E., Cameron, P.L., Maycox, P.R., Baumert, M., Lottspeich, F., De Camilli, P., and Jahn, R. (1989). Synaptic vesicles immunoisolated from rat cerebral cortex contain high levels of glutamate. Neuron *3*, 715–720.

Camilli, P.D.E., Harris, S.M., Huttner, W.B., and Greengard, P. (1983). Synapsin I (Protein I), a Nerve Terminal-Specific Phosphoprotein . II . Its Specific Association with Synaptic Vesicles Demonstrated by Immunocytochemistry in Agarose-embedded Synaptosomes. J. Cell Biol. *96*, 1355–1373.

Cash, D. (1994). Gammahydroxybutyrate : An Overview of the Pros and Cons for it Being a Neurotransmitter And / Or a Useful Therapeutic Agent. Neurosci. Biobehav. Rev. *18*, 291–304.

Chantranupong, L., Scaria, S.M., Saxton, R.A., Harper, J.W., Gygi, S.P., Sabatini, D.M., Chantranupong, L., Scaria, S.M., Saxton, R.A., Gygi, M.P., et al. (2016). The CASTOR Proteins Are Arginine Sensors for the The CASTOR Proteins Are Arginine Sensors. Cell 1–12.

Chen, W.W., Freinkman, E., Wang, T., Birsoy, K., and Sabatini, D.M. (2016). Absolute Quantification of Matrix Metabolites Reveals the Dynamics of Mitochondrial Metabolism. Cell *166*, 1324-1337.e11.

Chen, W.W., Freinkman, E., and Sabatini, D.M. (2017). Rapid immunopurification of mitochondria for metabolite profiling and absolute quantification of matrix metabolites. Nat. Protoc. *12*, 2215–2231.

Clarke, M.C., and Haig, D.A. (1971). Taurine-a Possible Neurotransmitter? Nature *234*, 107–108.

Cox, J., and Witten, I.B. (2019). Striatal circuits for reward learning and decision-making. Nat. Rev. Neurosci. *20*, 482–494.

Craige, B., Salazar, G., and Faundez, V. (2004). Isolation of Synaptic Vesicles (John Wiley & Sons, Inc.).

Damier, P., Hirsch, E.C., Agid, Y., and Graybiel, A.M. (1999). The substantia nigra of the human brain II .

825 Patterns of loss of dopamine-containing neurons in Parkinson ' s disease. Brain *122*, 1437–1448.
826 Daubner, S.C., Le, T., and Wang, S. (2011). Tyrosine hydroxylase and regulation of dopamine synthesis.
827 Arch. Biochem. Biophys. *508*, 1–12.
828 Dulcis, D., Jamshidi, P., Leutgeb, S., and Spitzer, N.C. (2013). Neurotransmitter switching in the adult
829 brain regulates behavior. Science (80-.). *340*, 449–453.
830 Durieux, P.F., Bearzatto, B., Guiducci, S., Buch, T., Waisman, A., Zoli, M., Schiffmann, S.N., and
831 Kerchove, A. De (2009). D2R striatopallidal neurons inhibit both locomotor and drug reward processes.
832 Nat. Neurosci. *12*, 2008–2010.
833 Edwards, R.H. (1992). The transport of neurotransmitters into synaptic vesicles. Curr. Opin. Neurobiol. *2*,
834 586–594.
835 Elsworth, J.D., and Roth, R.H. (1997). Dopamine Synthesis, Uptake, Metabolism, and Receptors :
836 Relevance to Gene Therapy of Parkinson's Disease. Exp. Neurol. *9*, 4–9.
837 Eng, J.K., Mccormack, A.L., and Yates, J.R. (1994). An Approach to Correlate Tandem Mass Spectral
838 Data of Peptides with Amino Acid Sequences in a Protein Database. Am. Soc. Mass Spectrom. *5*, 976–
839 989.
840 Erickson, J.D., Schxfert, M.K., Bonner, T.O.M.I., Eiden, L.E.E.E., and Weihet, E. (1996). Distinct
841 pharmacological properties and distribution in neurons and endocrine cells of two isoforms of the human
842 vesicular monoamine transporter. Proc. Natl. Acad. Sci. *93*, 5166–5171.
843 Eshkind, L.G., and Leube, R.E. (1995). Mice lacking synaptophysin reproduce and form typical synaptie
844 vesicles. Cell Tissue Res. *282*, 423–433.
845 Fernandez, C.A., Rosiers, C. Des, Previs, S.F., David, F., and Brunengrabert, H. (1996). Correction of 3C
846 Mass Isotopomer Distributions for Natural Stable Isotope Abundance. J. Mass Spectrom. *31*, 255–262.
847 Fleck, M.W., and Palmerv, A.M. (1993). Aspartate and Glutamate Mediate in Area CA1 of the
848 Hippocampus Excitatory Synaptic Transmission. J. Neurosci. *13*, 3944–3955.
849 Franchi, S.A., Macco, R., Astro, V., Tonoli, D., and Savino, E. (2018). A Method to Culture GABAergic
850 Interneurons Derived from the Medial Ganglionic Eminence. Front. Cell. Neurosci. *11*, 1–21.
851 Fremeau Jr, R.T., Troyer, M.D., Pahner, I., Nygaard, G.O., Tran, C.H., Reimer, R.J., Bellocchio, E.E.,
852 Fortin, D., Storm-mathisen, J., and Edwards, R.H. (2001). The Expression of Vesicular Glutamate
853 Transporters Defines Two Classes of Excitatory Synapse University of Oslo. Neuron *31*, 247–260.
854 Gondré-lewis, M.C., Park, J.J., and Loh, Y.P. (2012). Cellular Mechanisms for the Biogenesis and
855 Transport of Synaptic and Dense-Core Vesicles (Elsevier).
856 Gronborg, M., Pavlos, N.J., Brunk, I., Chua, J.J.E., Munster-Wandowski, A., Riedel, D., Ahnert-Hilger, G.,
857 Urlaub, H., and Jahn, R. (2010). Quantitative Comparison of Glutamatergic and GABAergic Synaptic
858 Vesicles Unveils Selectivity for Few Proteins Including MAL2, a Novel Synaptic Vesicle Protein. J.
859 Neurosci. *30*, 2–12.
860 Gundersen, R.Y., Vaagenes, P., Breivik, T., Fonnum, F., and Opstad, P. (2005). Glycine - an important
861 neurotransmitter and cytoprotective agent. Acta Anaesthesiol Scand *49*, 1108–1116.

Herring, B.E., Silm, K., Edwards, R.H., and Nicoll, R.A. (2015). Is Aspartate an Excitatory Neurotransmitter? J. Neurosci. *35*, 10168–10171.

Hnasko, T.S., and Edwards, R.H. (2012). Neurotransmitter corelease: mechanism and physiological role. Annu. Rev. Physiol. *74*, 225–243.

Huang, K.W., Ochandarena, N.E., Philson, A.C., Hyun, M., Birnbaum, J.E., Cicconet, M., and Sabatini, B.L. (2019). Molecular and anatomical organization of the dorsal raphe nucleus. Elife *8*, 1–34.

Huttlin, E.L., Ting, L., Raphael, J., Paulo, J.A., Wade, J., Gygi, S.P., Huttlin, E.L., Ting, L., Bruckner, R.J., Gebreab, F., et al. (2015). The BioPlex Network : A Systematic Exploration of the Human Interactome. Cell *162*, 425–440.

Huttner, W.B., Schiebler, W., Greengard, P., and De Camilli, P. (1983). Synapsin I (Protein I), a Nerve Terminal-Specific Phosphoprotein. III. Its Association with Synaptic Vesicles Studied in a Highly Purified Synaptic Vesicle Preparation. J. Cell Biol. *96*, 1374–1388.

Jackman, S.L., Beneduce, B.M., Drew, I.R., and Regehr, W.G. (2014). Achieving High-Frequency Optical Control of Synaptic Transmission. J. Neurosci. *34*, 7704–7714.

Jackman, S.L., Turecek, J., Belinsky, J.E., and Regehr, W.G. (2016). The calcium sensor synaptotagmin 7 is required for synaptic facilitation. Nature *529*, 88–91.

Jahn, R., and Sudhof, T.C. (1994). Synaptic vesicles and exocytosis. Annu. Rev. Neurosci. *17*, 219–246.

Jonas, P., Bischofberger, J., and Sandkühler, J. (1998). Corelease of two fast neurotransmitters at a central synapse. Science *281*, 419–424.

Jones E, Oliphant E, Peterson P, et al. SciPy: Open Source Scientific Tools for Python.

Kanazawa, H., and Wada, Y.O.H. (2000). Luminal acidification of diverse organelles by V-ATPase in animal cells. J. Exp. Biol. *203*, 107–116.

Kilb, W., and Fukuda, A. (2017). Taurine as an Essential Neuromodulator during Perinatal Cortical Development. Front. Cell. Neurosci. *11*, 1–13.

Kim, J.-I., Ganesan, S., Luo, S.X., Wu, Y.-W., Park, E., Huang, E.J., Chen, L., and Ding, J.B. (2015). Aldehyde dehydrogenase 1a1 mediates a GABA synthesis pathway in midbrain dopaminergic neurons. Science (80-.). *350*, 102–106.

Kugler, S., Kilic, E., and Bahr, M. (2003). Human synapsin 1 gene promoter confers highly neuron-specific long-term transgene expression from an adenoviral vector in the adult rat brain depending on the transduced area. Gene Ther. *10*, 337–347.

Lammel, S., Elizabeth, E., Luo, L., Robert, C., Wall, N.R., Beier, K., and Luo, L. (2015). Diversity of Transgenic Mouse Models for Selective Targeting of Midbrain Dopamine Neurons. Neuron *85*, 429–438.

Lei, Z., Huhman, D. V, and Sumner, L.W. (2011). Mass Spectrometry Strategies in Metabolomics. J. Biol. Chem. *286*, 25435–25442.

Lewis, C.A., Parker, S.J., Fiske, B.P., Mccloskey, D., Gui, D.Y., Green, C.R., Vokes, N.I., Feist, A.M., Heiden, M.G. Vander, and Metallo, C.M. (2014). Tracing Compartmentalized NADPH Metabolism in the Cytosol and Mitochondria of Mammalian Cells. Mol. Cell *55*, 253–263.

Love, M.I., Huber, W., and Anders, S. (2014). Moderated estimation of fold change and dispersion for RNA-seq data with DESeq2. Genome Biol. *15*, 1–21.

Lynch, B.A., Lambeng, N., Nocka, K., Kensel-Hammes, P., Bajjalieh, S.M., Matagne, A., and Fuks, B. (2004). The synaptic vesicle protein SV2A is the binding site for the antiepileptic drug levetiracetam. Proc. Natl. Acad. Sci. U. S. A. *101*, 9861–9866.

Macdonald, R.L. (1994). GABA A receptor channels. Annu. Rev. Neurosci. *17*, 569–602.

Mariani, M., Camagna, M., Tarditi, L., and Seccamani, E. (1991). A new enzymatic method to obtain high-yield F(ab)2 suitable for clinical use from mouse IgGl. Mol. Immunol. *28*, 69–77.

Mathews, G.C., and Diamond, J.S. (2003). Neuronal Glutamate Uptake Contributes to GABA Synthesis and Inhibitory Synaptic Strength. J. Neurosci. *23*, 2040–2048.

Mickelsen, L.E., Iv, F.W.K., Chimileski, B.R., Fujita, A., Norris, C., Nelson, C.E., and Jackson, A.C. (2017). Neurochemical Heterogeneity Among Lateral Hypothalamic Hypocretin / Orexin and Melanin-Concentrating Hormone Neurons Identified Through Single-Cell Gene Expression Analysis. ENeuro *4*, 1–24.

Nagy, A., Baker, R.R., Morris, S.J., and Whittaker, V.P. (1976). The preparation and characterization of synaptic vesicles of high purity. Brain Res. *109*, 285–309.

Nicoll, A., Malenka, C., Kauer, A., and Francisco, S. (1990). Functional Comparison of Neurotransmitter Receptor Subtypes in Mammalian Central Nervous System. Physiol. Rev. *70*, 514–549.

Nishiyama, J., Mikuni, T., and Yasuda, R. (2017). Virus-Mediated Genome Editing via Homology-Directed Repair in Mitotic and Postmitotic Cells in Mammalian Brain. Neuron *96*, 755-768.e5.

Olbrich, H., and Braak, H. (1985). Anatomy and Embryology Ratio of pyramidal cells versus non-pyramidal cells in sector CA1 of the human Ammon's horn. Anat Embryol *173*, 105–110.

Pacold, M.E., Brimacombe, K.R., Chan, S.H., Rohde, J.M., Lewis, C.A., Swier, L.J.Y.M., Possemato, R., Chen, W.W., Sullivan, L.B., Fiske, B.P., et al. (2016). A PHGDH inhibitor reveals coordination of serine synthesis and one-carbon unit fate. Nat. Chem. Biol. *12*, 452–462.

Parker, S.J., Svensson, R.U., Divakaruni, A.S., Lefebvre, A.E., Murphy, A.N., Shaw, R.J., and Metallo, C.M. (2017). LKB1 promotes metabolic flexibility in response to energy stress. Metab. Eng. *43*, 208–217.

Patneau, K., and Mayer, L. (1990). Structure-Activity Relationships for Amino Candidates Acting at N-Methyl-D-Aspartate Receptors Acid Transmitter and Quisqualate Receptors. J. Neurosci. *10*, 2385–2399.

Patti, G., Yanes, O., and Siuzdak, G. (2012). Innovation: Metabolomics: the apogee of the omics trilogy. Nat. Publ. Gr. *13*, 263–269.

Peng, J., and Gygi, S.P. (2001). Proteomics : the move to mixtures. J. Mass Spectrom. *36*, 1083–1091.

Pines, G., Danboltt, N.C., Bj, M., Zhang, Y., Bendahan, A., Eide, L., Koepsellll, H., Storm-mathisent, J., Seeberg, E., and Kanner, B.I. (1992). Cloning and expression of a rat brain L-glutamate transporter. Nature *360*, 464–467.

Pisoni, R.L., and Thoene, J.G. (1991). The transport systems of mammalian lysosomes. Biochim. Biophys. Acta *1071*, 351–373.

Ray, G.J., Boydston, E.A., Shortt, E., Wyant, G.A., Chen, W.W., and Sabatini, D.M. (2020). A PEROXO-Tag enables rapid isolation of peroxisomes from human cells. ISCIENCE 101109.

Reis, D.J., and Regunathan, S. (2000). Is agmatine a novel neurotransmitter in brain ? TiPS *21*, 31–34.

Rizzoli, S.O., and Betz, W.J. (2005). Synaptic vesicle pools. Nat. Rev. Neurosci. *6*, 57–69.

Root, D.H., Mejias-Aponte, C.A., Zhang, S., Wang, H.-L., Hoffman, A.F., Lupica, C.R., and Morales, M. (2014). Single rodent mesohabenular axons release glutamate and GABA. Nat. Neurosci. *17*, 1543–1551.

Saunders, A., Granger, A.J., Sabatini, B.L., and Nelson, S.B. (2015). Corelease of acetylcholine and GABA from cholinergic forebrain neurons. Elife *4*, e06412.

Scherman, D., Jaudon, P., and P, H.J. (1983). Characterization of the monoamine carrier of chromaffin granule membrane by binding of [2-3H]dihydrotetrabenazine. Proc. Natl. Acad. Sci. *80*, 584–588.

Schousboe, A., Bak, L.K., and Waagepetersen, H.S. (2013). Astrocytic control of biosynthesis and turnover of the neurotransmitters glutamate and GABA. Front. Endocrinol. (Lausanne). *4*, 1–11.

Sciarretta, C., and Minichiello, L. (2010). The Preparation of Primary Cortical Neuron Cultures and a Practical Application Using Immunofluorescent Cytochemistry. In Mouse Cell Culture: Methods and Protocols, A. Ward, and D. Tosh, eds. (Totowa, NJ: Humana Press), pp. 221–231.

Shabel, S.J., Proulx, C.D., Piriz, J., and Malinow, R. (2014). Mood regulation. GABA/glutamate co-release controls habenula output and is modified by antidepressant treatment. Science (80-.). *345*, 1494–1498.

Smith, C.A., Maille, G.O., Want, E.J., Qin, C., Trauger, S.A., Brandon, T.R., Custodio, D.E., Abagyan, R., and Siuzdak, G. (2005). METLIN: A Metabolite Mass Spectral Database. Ther. Drug Monit. *27*.

Sobolevsky, T., Revelsky, A., Miller, B., Oreido, V., Chernetsova, E.S., and Revelsky, I. (2003). Comparison of silylation and esterification / acylation procedures in GC-MS analysis of amino acids. J. Sep. Sci. *26*, 1474–1478.

Spitzer, N.C. (2012). Activity-dependent neurotransmitter respecification. Nat. Rev. Neurosci. *13*, 94–106.

Stenerson, K. (2011). The Derivatization and Analysis of Amino Acids by GC-MS. Sigma-Aldrich *25*, 9–11.

Strata, P., and Harvey, R. (1999). Dale's principle. Brain Res. Bull. *50*, 349–350.

Südhof, T.C. (2013). A molecular machine for neurotransmitter release : synaptotagmin and beyond. Nat. Publ. Gr. *19*, 1227–1231.

Takamori, S., Rhee, J.S., Rosenmund, C., and Jahn, R. (2001). Identification of Differentiation-Associated Brain-Specific Phosphate Transporter as a Second Vesicular Glutamate Transporter (VGLUT2). J. Neurosci. *21*, 1–6.

Takamori, S., Holt, M., Stenius, K., Lemke, E.A., Grønborg, M., Riedel, D., Urlaub, H., Schenck, S., Brügger, B., Ringler, P., et al. (2006). Molecular Anatomy of a Trafficking Organelle. Cell *127*, 831–846.

Tiedje, K.E., Stevens, K., Barnes, S., and Weaver, D.F. (2010). Beta-Alanine as a small molecule neurotransmitter. Neurochem. Int. *57*, 177–188.

Trapp, X.S., and Cork, S.C. (2020). PPG neurons of the lower brain stem and their role in brain GLP-1

receptor activation. Am J Physiol Regul Integr Comp Physiol 309 *309*, 795–804.

Traynelis, S.F., Wollmuth, L.P., Mcbain, C.J., Menniti, F.S., Vance, K.M., Ogden, K.K., Hansen, K.B., Yuan, H., Myers, S.J., and Dingledine, R. (2014). Glutamate Receptor Ion Channels : Structure, Regulation, and Function. Pharmacol. Rev. *10*, 405–496.

Tritsch, N.X., Ding, J.B., and Sabatini, B.L. (2012). Dopaminergic neurons inhibit striatal output through non-canonical release of GABA. Nature *490*, 262–266.

Tritsch, N.X., Granger, A.J., and Sabatini, B.L. (2016). Mechanisms and functions of GABA co - release. Nat. Rev. Neurosci. 1–7.

Vergnano, A.M., Rebola, N., Savtchenko, L.P., Pinheiro, P.S., Casado, M., Kieffer, B.L., Rusakov, D.A., Mulle, C., and Paoletti, P. (2014). Zinc dynamics and action at excitatory synapses. Neuron *82*, 1101–1114.

Voge, N. V, Perera, R., Mahapatra, S., Gresh, L., Balmaseda, A., Loro, M.A., Hopf-jannasch, A.S., Belisle, J.T., Harris, E., Blair, C.D., et al. (2016). Metabolomics-Based Discovery of Small Molecule Biomarkers in Serum Associated with Dengue Virus Infections and Disease Outcomes. Plos 1–27.

Vong, L., Ye, C., Yang, Z., Choi, B., Chua, S., and Lowell, B.B. (2011). Leptin Action on GABAergic Neurons Prevents Obesity and Reduces Inhibitory Tone to POMC Neurons. Neuron *71*, 142–154.

Wenig, P., and Odermatt, J. (2010). OpenChrom : a cross-platform open source software for the mass spectrometric analysis of chromatographic data.

Wojcik, S.M., Katsurabayashi, S., Guillemin, I., Friauf, E., Rosenmund, C., and Brose, N. (2006). A Shared Vesicular Carrier Allows Synaptic Corelease of GABA and Glycine. Neuron *4*, 575–587.

Yelin, R., and Schuldiner, S. (1995). The pharmacological profile of the vesicular monoamine transporter resembles that of multidrug transporters. FEBS *377*, 201–207.

Yoshida, M., and Precht, W. (1971). Monosynaptic inhibition of neurons of the substantia nigra by caudatonigral fibers. Brain *32*, 225–228.

Zhang, S., Qi, J., Li, X., Wang, H.-L., Britt, J.P., Hoffman, A.F., Bonci, A., Lupica, C.R., and Morales, M. (2015). Dopaminergic and glutamatergic microdomains in a subset of rodent mesoaccumbens axons. Nat. Neurosci. *18*, 386–392.

Zhou, F., Wilson, C.J., and Dani, J.A. (2002). Cholinergic Interneuron Characteristics and Nicotinic Properties in the Striatum. J Neurobiol *53*, 590–605.